

This is to certify that the

dissertation entitled

Global Active Noise Control of a One-Dimensional Acoustic  
Duct Using a Feedback Controller

presented by

Andrew James Hull

has been accepted towards fulfillment  
of the requirements for

Ph.D. degree in Mechanical Engineering

*Clark Padelford*  
Major professor

Date May 4, 1990



PLACE IN RETURN BOX to remove this checkout from your record.  
TO AVOID FINES return on or before date due.

DATE DUE	DATE DUE	DATE DUE
FEB 07 1994 6 3 0 3 3	_____	_____
<del>JUN 13 1994</del>	_____	_____
SEP 23 1994	_____	_____
284	_____	_____
_____	_____	_____
_____	_____	_____
_____	_____	_____
_____	_____	_____

MSU Is An Affirmative Action/Equal Opportunity Institution

**GLOBAL ACTIVE NOISE CONTROL OF A ONE-DIMENSIONAL  
ACOUSTIC DUCT USING A FEEDBACK CONTROLLER**

By

**Andrew James Hull**

**A DISSERTATION**

Submitted to  
Michigan State University  
in partial fulfillment of the requirements  
for the degree of

**DOCTOR OF PHILOSOPHY**

Department of Mechanical Engineering

1990

605562X

## **ABSTRACT**

### **GLOBAL ACTIVE NOISE CONTROL OF A ONE-DIMENSIONAL ACOUSTIC DUCT USING A FEEDBACK CONTROLLER**

By

**Andrew James Hull**

Active noise control of acoustic enclosures is a classical engineering problem. The active noise control of a one-dimensional hard-walled duct with a partially dissipative boundary condition is addressed in this dissertation. Previous techniques have attacked this problem by developing adaptive filters to decrease the noise level at a single measurement location; they ignore the problem of noise reduction at other locations in the duct. The work presented here applies classical control theory to reduce noise levels in a one-dimensional acoustic enclosure. Classical control theory provides a basis to reduce the noise levels in the duct globally, rather than at a single location. This is accomplished by adding a response measurement microphone and a control speaker to the open loop system. Pressure measurements are taken at a single location and passed to an observer, which provides state estimates of the system. Once the state estimates are known, a pole placement control algorithm is used to lower the noise level. Pole placement produces noise control globally, rather than at a single location. Experimental result obtained here show that the noise level in the duct can be reduced by 55% when the system is excited by random noise excitation.

## **Copyright**

Copyright by

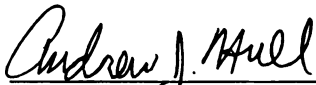
**Andrew James Hull**

1990

### Certification

This is to certify that the dissertation entitled  
**Global Active Noise Control of a One-Dimensional Acoustic  
Duct Using a Feedback Controller**

presented by



Andrew J. Hull  
DOCTOR OF PHILOSOPHY Candidate

5/15/90

Date


has been accepted towards fulfillment of the requirements for a  
DOCTOR OF PHILOSOPHY DEGREE in Mechanical Engineering at  
Michigan State University  
by



Clark J. Radcliffe  
Associate Professor, Dissertation Advisor

5/3/90

Date



Charles R. MacCluer  
Professor, Dept. of Mathematics

5/14/90

Date



Alan G. Haddow  
Assistant Professor, Dept. of Mechanical Engineering

5/14/90

Date



H. Roland Zapp  
Associate Professor, Dept. of Electrical Engineering

5/14/90

Date

## **Acknowledgements**

I would like to express my sincere appreciation to my advisor Clark Radcliffe, for helping me all the way through the dissertation. His guidance was always positive even in the darkest of dissertation times. Additionally I would like to thank Chuck MacCluer for his help and insight in the theoretical areas of the dissertation.

I would like to thank my committee members Roland Zapp and Alan Haddow for their comments concerning the dissertation. Also I would like to thank Milan Miklavcic, J.C. Kurtz, Erik Goodman and Robert Soutas-Little, all of whom were helpful in one way or another. I would like to thank Bob Rose and Leonard Eisele who made the complicated fixtures necessary for the experiments in this work.

I would like to thank my mother, brother and sister for their encouragement when I was in graduate school.

I would like to thank my officemate, Steve Southward for his friendship over the years and his understanding of this problem. I would like to thank Mark Barlow for helping me with the development of the digital signal processing code. Finally I would like to thank my friends from around the East Lansing area over the past five years. They include: Bashar AbdulNour, Guy Allen, Jeff Beranek, Teresa Brown, Dave Butcher, Yossi Chait, Greg Fell, Eva-Marie Fadel, Jane Hawkins, Jon Hickey, Dave Miner, Jim Oliver, Ace Sannier, and Shawna Sannier among others.





## **Table of Contents**

List of Tables	viii
List of Figures	ix
Chapter 1 - Introduction	1
1.1 Overview	1
1.2 A New Control Technique	2
1.3 Chapter Summary	2
Chapter 2 - State Space Model Representation	5
2.1 Introduction	5
2.2 System Model	6
2.3 Separation of Variables	8
2.4 Series Solution	10
2.5 A New Inner Product	15
2.6 State Space Formulation	17
2.7 Frequency Response	18
2.8 Accuracy of Truncated Solution	19
2.9 Transient Response	21
Chapter 3 - Experimental Verification of the State Space Model	26
3.1 Model Verification Experiment	26
3.2 Pressure Excitation, Constant Acoustic Impedance	26
3.3 Mass Flow Excitation, Constant Acoustic Impedance	29
3.4 Pressure Excitation, Nonconstant Acoustic Impedance	29
3.5 Transient Response	34

Chapter 4 - Acoustic Impedance Measurement	38
4.1 Introduction	38
4.2 System Model and System Eigenvalues	39
4.3 Acoustic Impedance Computation	41
4.4 Acoustic Impedance Measurement Experiment	44
Chapter 5 - State Estimation	53
5.1 Introduction	53
5.2 Observer Equations	55
5.3 Observer Gain Placement	56
5.4 Closed Form Solution	58
5.5 Numerical Simulations for Continuous Time Observers	61
5.6 Numerical Simulations for a Discrete Time Observer	65
Chapter 6 - Active Noise Control	68
6.1 Active Noise Control Using Pole Placement	68
6.2 Controller Equations	68
6.3 Control Gain Placement	69
6.4 Frequency Domain Simulations	70
6.5 Time Domain Simulations	76
6.6 Actuator Dynamics	78
6.7 Active Noise Control Experiment	80
Chapter 7 - Conclusions	86
7.1 Dissertation Summary	86
7.2 Directions for Future Work	87
Appendix. Wave Equation Derivation	89
Bibliography	91

## **List of Tables**

<b>Table</b>	<b>Page</b>
3.1 <b>Calculated Acoustic Impedance.</b>	<b>32</b>
4.1 <b>Measured Duct Eigenvalues for the Foam End.</b>	<b>49</b>
4.2 <b>Calculated Acoustic Impedance for the Foam End.</b>	<b>49</b>
4.3 <b>Measured Duct Eigenvalues for the Capped End.</b>	<b>51</b>
4.4 <b>Calculated Acoustic Impedance for the Capped End.</b>	<b>51</b>

## List of Figures

Figure	Page
2.1 Third Eigenfunction for Duct Particle Displacement with End Impedances: K = .5+0i and K = 0+0i.	11
2.2 Third Eigenfunction for Duct Particle Displacement with End Impedances: K = 0+3.0i and K = 0+0i.	12
2.3 Third Eigenfunction for Duct Particle Displacement with End Impedances: K = 0.8+0.5i and K = 0+0i.	13
2.4 End-Point (x=0) Pressure Excited Steady State Frequency Response with an Impedance Constant of K = 0.3+0.2i at x = 0.4267 m.	22
2.5 Frequency Response Truncation Error of an 11 Term Model with Impedance Constant of K = 0.3+0.2i.	23
2.6 Interior Point Mass Flow Excited Steady State Frequency Response with an Impedance Constant of K=0.3+0.2i at x=0.4267 m. Excitation at $x_1=1.22$ m.	24
2.7 Harmonic Time Response of 5 and 51 Term Duct Models with an Impedance Constant of K = 0.3+0.2i.	25
2.8 Pulse Time Response of a 1.5 m Duct with an End Impedance of K = 0.3+0i.	25
3.1 Laboratory Configuration.	27
3.2 Frequency Response of Duct with End Pressure Excitation.	28
3.3 Frequency Response of Duct with Interior Mass Flow Excitation.	30
3.4 Frequency Response of Duct with Nonconstant Acoustic Impedance.	33
3.5 System Pressure Input at x=0.	36
3.6 Transient Response of Duct at x=0.792 m with 51 Terms.	36
3.7 Transient Response of Duct with 21 Terms.	37
3.8 Transient Response of Duct with 15 Terms.	37

4.1	System Eigenvalues $\Lambda_n$ , for Constant K.	42
4.2	Laboratory Configuration.	45
4.3	Frequency Response of Duct with Foam End at $x=0.792$ m.	50
4.4	Frequency Response of Duct with Closed End at $x=0.792$ m.	52
5.1	Observer and Duct Diagram (Chen, 1984).	54
5.2	Duct with Observer and Input Speaker.	55
5.3	Closed Form Solution of Duct Pressure Calculated by Observer Compared with Steady State Duct Model Response.	60
5.4	Integrated Observer Solution and Model Duct Response.	62
5.5	Integrated Observer Solution and Model Duct Response. Nonzero Initial Conditions Showing Robustness of Observer Design.	63
5.6	State Estimate $a_1(t)$ .	64
5.7	Discrete Time Observer Solution and Model Duct Response.	67
6.1	Active Noise Control System.	69
6.2	Plant and Control System.	70
6.3	Closed and Open Loop Frequency Response, Compensator at $x=3.56$ m.	73
6.4	Closed and Open Loop Frequency Response, Compensator at $x=1.37$ m.	74
6.5	Closed and Open Loop frequency Response, Showing Change of Natural Frequency of System.	75
6.6	Time Domain Response with Modeled Disturbance.	77
6.7	Time Domain Response with Unmodeled Disturbance.	78
6.8	Actuator Magnitude and Phase Plots.	79
6.9	Experimental Frequency Response, First Mode.	83
6.10	Experimental Frequency Response, Second Mode.	84
6.11	First Mode Response.	85
6.12	Second Mode Response.	85
A.1	Duct with Section $dx$ .	90



**That which does not kill us will surely make us strong**

**Nietzsche, F., circa 1800**

## **Chapter 1. Introduction**

### **1.1. Overview**

Active noise control can produce quieter environments that are safer, more productive, and more comfortable. In work areas such as power plants, factories, and offices that contain long duct assemblies, reduction of sound energy in the ducts generated by fans and other machinery is often required. The advantages of reducing noise levels is evident, and recently more communities have passed legislation to limit excessive noise. Passive techniques such as the use of absorbent materials have little effect on low frequency noise, and then active noise controllers are required. Passive techniques are also difficult if not impossible to install in many acoustic environments.

An active noise control system in a duct usually consists of one or more cancellation speakers driven by an algorithm designed to reduce noise levels. The duct normally has one or more signal microphones at some location while noise is driven by excitation through one end. A variety of different active noise suppression schemes have been developed in recent years (Swinbanks, 1973; Ross, 1981; Trinder and Nelson, 1983; LaFontaine and Shepherd, 1983; Tichy et al., 1984; Roure, 1985; Mollo and Bernhard, 1987; Eriksson et al., 1988; Manjal and Eriksson, 1988; Warner et al., 1988). The control techniques used in these studies are some type of adaptive filter which cancels noise at a specific measurement location. The response at areas other than the measurement location is either ignored or not measured and typically is increased. These studies have not used classical feedback control theory and the wealth of design and stability theorems this theory provides. Feedback control can provide global noise reduction to the system, unlike

previous studies whose noise reduction has been limited to one point or a small region of the duct.

## **1.2. A New Control Technique**

The objective of the research discussed here is the application of classical pole placement to achieve active noise control in a duct. Pole placement modifies the eigenstructure of the system to increase the dissipation of the duct and attenuate duct noise. This dissertation develops a control technique for a one-dimensional hard-walled duct with a control speaker at some location, a totally reflective entrance boundary condition, and a partially absorptive termination boundary condition. The effect of the partially absorptive boundary condition is to allow propagating and standing wave responses to exist in the duct simultaneously. These two wave characteristics yield eigenvalues with eigenfunctions that are not orthogonal on the interval of the length of the duct with respect to the ordinary inner product. This is unlike previous discretized acoustic models which considered only idealized reflecting boundary conditions.

Analogous problems which have propagating and standing wave characteristics coexisting in the system include circular saw blades, large scale space structures, turbine wheels, robot arms and electrical transmission lines with resistive loads. Understanding the acoustic problem stated here can lead to a better understanding of these analogous systems. Additionally, the first step in building any generalized three-dimensional control system is a thorough understanding the one-dimensional control problem.

## **1.3. Chapter Summary**

Chapter 2 develops the state space model for the acoustic duct. State space model representation for the system is required to apply classical pole placement to the duct. The

model is derived from separation of variables. Due to the nonself-adjoint boundary condition, traditional methods of orthogonal mode shapes cannot be applied to this problem. The separation of variables problem is transferred onto a different interval, where the time and space modes are decoupled. The problem is then transferred back onto the original interval, where the state space model results.

Chapter 3 describes an experimental verification of the state space model. Experimental verification of the state space model is essential if real time control is to be applied to the duct. Steady state verification of end excitation and domain excitation are presented for a frequency constant termination end. The problem of frequency dependent terminations is discussed and an experiment incorporating this behavior is shown. The transient solution to the duct is also experimentally verified.

Chapter 4 develops a measurement technique to determine the boundary condition on the termination end of the duct. This is accomplished by taking the system eigenvalue equation and solving the inverse problem for the acoustic impedance. This measurement technique is experimentally verified and the stability of the measurement method is discussed.

Chapter 5 develops a state estimation method using observer theory. This is necessary since the feedback control system needs a knowledge of the system states, which are not measurable directly. They can be estimated, however, by measuring the pressure at some location in the duct which is used to drive a state estimator. The state estimator requires real time integration, and the effects of four different integration routines is benchmarked and discussed.

Chapter 6 develops a pole placement control algorithm for the duct. Frequency and time domain simulations are shown. The effects of nonideal control actuators is discussed. Active noise control is demonstrated experimentally. The effect of control from a

frequency domain standpoint is shown. Global noise attenuation is verified. System stability and instability is discussed.

Chapter 7 summarizes this dissertation. Directions for future research are discussed.

## Chapter 2. State Space Model Representation\*

### 2.1. Introduction

The dynamic response of an enclosed acoustic system is determined by both the governing differential equations and associated boundary conditions. The modeling of one-dimensional acoustic response is a classical engineering problem (Rayleigh, 1878). The response of hard-walled ducts with idealized reflecting and/or nonreflecting terminations to point source excitation has been developed previously (Snowdon, 1971; Doak, 1973a; Swinbanks, 1973; Trinder and Nelson, 1983; Tichy et al., 1984). Models of ducts with idealized totally reflective boundary conditions yield self-adjoint differential operators and are easily discretized from their mutually orthogonal modes. Models of ducts with totally absorbent boundary conditions do not resonate, so wave propagation models are used.

Actual acoustic systems have non-idealized, partially reflective boundary conditions, yielding some combination of propagating and standing wave components in their acoustic pressure response (Davis et al., 1954; Spiekermann, 1986; Spiekermann and Radcliffe, 1988a, 1988b). Nonreflecting terminations in linear systems result in propagating wave response while reflecting terminations result in standing wave response. Currently available analytical model solutions do not take into account the possibility that the acoustic response could be a combination of standing and propagating waves nor do they consider the effect of partially absorptive boundary conditions on duct models. The

---

\* This chapter is based on the paper "State Space Representation of the Nonself-Adjoint Acoustic Duct System," accepted for publication in the *ASME Journal of Vibration and Acoustics*.



partially absorptive boundary condition produces a nonself-adjoint differential operator. Traditional methods of orthogonal mode shape discretization for this class of problems cannot be applied because the eigenfunctions are not orthogonal with the conventional inner product over the domain of the operator and the conventional eigenfunction inner product does not decouple the model's state equations. Nonself-adjoint operators may yield non-conjugate, complex eigenvalues. Physically, the nonself-adjoint model results from energy propagation down the duct and out the end.

This chapter develops an infinite order, diagonal, state space model of a duct with a partially absorptive boundary condition. The model is intended for future development of a time domain control theory since time domain control of high order systems frequently uses state observers designed from state space system models. The analysis diagonalizes the state space model; past work (Chait et al., 1988) has shown that diagonalized system equations provide more accuracy when truncated than models which include off-diagonal terms. The results here may also contribute to methods for evaluating duct end point impedances and other issues in the development of duct designs.

## 2.2. System Model

The system model is of a one-dimensional hard-walled duct excited by a pressure input at one end, a partially reflective boundary condition at the other end, and an arbitrary number of mass flow inputs in the domain. This partially reflective boundary condition allows the acoustic response model to include standing and propagating wave responses simultaneously. The partially reflective condition in the duct allows some energy to be dissipated out the end while the rest is reflected back into the system producing a bounded complex system response from a nonself-adjoint differential operator.



The linear second order wave equation modeling particle displacement in a hard-walled, one-dimensional duct is (Seto, 1971; Doak, 1973b)

$$\frac{\partial^2 u(x,t)}{\partial t^2} - c^2 \frac{\partial^2 u(x,t)}{\partial x^2} = - \frac{\partial}{\partial x} \left[ \frac{\delta(x)P(t)}{\rho} \right] - \sum_{i=1}^k [\delta(x - x_i)] \frac{\partial}{\partial t} \left[ \frac{M_i(t)}{\rho S} \right] \quad (2.1)$$

where  $u(x,t)$ =particle displacement (m),  $c$ =wave speed (m/s),  $x$ =spatial location (m),  $t$ =time (s),  $\rho$ =density of the medium ( $\text{kg/m}^3$ ),  $M_i(t)$ =mass flow input in the domain ( $\text{kg/s}$ ),  $x_i$ =location of mass flow input (m),  $S$ =speaker area driving the mass flow input ( $\text{m}^2$ ),  $P(t)$ =pressure excitation at  $x=0$  ( $\text{N/m}^2$ ), and  $\delta(x)$ =the Dirac delta function. The wave equation assumes an adiabatic system, no mean flow in the duct, uniform duct cross section and negligible air viscosity effects. The hard-wall assumption models the duct as having dissipation only at the termination end. The one-dimensional assumption requires the diameter of the duct to be small compared to its length. The duct's mean flow Mach number is assumed to be much less than one.

The partially reflective boundary condition model at location  $x=L$  is the relationship between the spatial gradient and the time gradient of particle displacement and is expressed as (Seto, 1973; Pierce, 1981; Spiekermann and Radcliffe, 1988a)

$$\frac{\partial u}{\partial x}(L,t) = -K \left( \frac{1}{c} \right) \frac{\partial u}{\partial t}(L,t) \quad K \neq 0+0i, 1+0i, \infty \quad (2.2)$$

where  $K$ =complex impedance of the termination end (dimensionless). Implicit in (2.2) is the acoustic analogy with electrical systems in which volume velocity is analogous to current and duct pressure is analogous to voltage. A second formulation called the reciprocal acoustic mobility analogy is also sometimes used; and if applied to this system, the parameter  $K$  in (2.2) would be the acoustic admittance. When  $\text{Re}(K)$  equals zero or is infinity, the termination end of the duct reflects all the acoustic energy and the response is composed of standing waves only. All other values of  $K$  yield some combination of

propagating and standing wave response (Spiekermann and Radcliffe, 1988a). When  $K=1+0i$  the termination end of the duct absorbs all the acoustic energy and the response is composed of propagating waves only. In general, the reflection coefficient  $(1-K)/(1+K)$  gives the relative magnitude of the reflected pressure wave. The real part of  $K$  (acoustic resistance) is associated with energy dissipation and is sometimes also called a loss coefficient, as it is a measure of the amount of energy leaving the duct. The imaginary part of  $K$  (acoustic reactance) is associated with conservative fluid compliance and/or inertia effects.

The duct end at  $x=0$  is modeled as a totally reflective, open end. This boundary condition is

$$\frac{\partial u}{\partial x}(0, t) = 0 \quad . \quad (2.3)$$

This corresponds to an open duct end (or an electrical short circuit). The acoustic pressure of the system is related to the spatial gradient of the particle displacement by (Seto, 1973)

$$P(x, t) = -\rho c^2 \frac{\partial u}{\partial x}(x, t) \quad . \quad (2.4)$$

The above four equations represent a mathematical model of the duct.

### 2.3. Separation of Variables

A decoupled series of ordinary differential equations in state space form which represent the wave equation are now developed. They will incorporate the boundary conditions (2.2-2.3) as well as initial conditions in the duct.

The eigenvalues and eigenfunctions of the model are found by applying separation of variables to (2.2-2.3) and the homogeneous version of (2.1). Separation of variables

assumes each term of the series solution is a product of a function in the spatial domain multiplied by a function in the time domain:

$$u(x, t) = X(x)T(t) \quad (2.5)$$

Substituting (2.5) into the homogeneous version of (2.1) produces two independent ordinary differential equations, each with complex valued separation constant  $\lambda$ , namely

$$\frac{d^2 X(x)}{dx^2} - \lambda^2 X(x) = 0 \quad (2.6)$$

and

$$\frac{d^2 T(t)}{dt^2} - \lambda^2 c^2 T(t) = 0 \quad (2.7)$$

The separation constant  $\lambda=0$  is a special case where  $X(x)=T(t)=1$  to satisfy (2.2) and (2.3).

The spatial ordinary differential equation (2.6) is solved for  $\lambda \neq 0$  using the boundary condition (2.3) yielding

$$X(x) = e^{\lambda x} + e^{-\lambda x} \quad (2.8)$$

The time dependent ordinary differential equation yields the following general solution

$$T(t) = Ae^{\lambda ct} + Be^{-\lambda ct} \quad (2.9)$$

Applying boundary condition (2.2) to (2.8) and (2.9) yields  $B=0$  and the separation constant

$$\lambda_n = \frac{1}{2L} \log_e \left( \frac{1-K}{1+K} \right) - \frac{n\pi i}{L}, \quad n = 0, \pm 1, \pm 2, \dots \quad (2.10)$$

Inserting the separation constant into (2.8) produces complex valued spatial eigenfunctions  $\varphi_n(x)$  where

$$\varphi_n(x) = e^{\lambda_n x} + e^{-\lambda_n x} \quad (2.11)$$

Unless the acoustic impedance  $K$  is zero or infinity, the eigenfunctions are not mutually orthogonal, conventional modal analysis of the original model (2.1) is not possible, and the time response cannot be found.

A typical eigenfunction for  $K$  real is shown in Figure 2.1. The solid line is the third ( $n=3$ ) eigenfunction for a partially reflective termination ( $K=0.5+0i$ ), and a duct length of 1.524 m (5 ft) used in previous studies (Spiekermann, 1986; Spiekermann and Radcliffe, 1988a, 1988b). The dashed line is the eigenfunction for the third ( $n=3$ ) mode with fully reflective duct termination ( $K=0+0i$ ). Note the real value of the eigenfunction with idealized reflecting termination,  $K=0+0i$ , and the complex value of the eigenfunction for  $K \neq 0$  (or  $1+0i$ ). Increasing the real part of  $K$  causes a shift in the magnitude of the eigenfunction near the termination and a rounding of the phase angles associated with increasing dissipation. A typical eigenfunction for  $K$  imaginary is shown in Figure 2.2. Increasing the imaginary part of  $K$  causes a spatial shift of the magnitude and the phase angle towards the termination. The relative magnitude of the eigenfunction remains unchanged. Figure 2.3 is an eigenfunction plot for  $K$  complex valued. It exhibits both characteristics of  $K$  real and  $K$  imaginary.

## 2.4. Series Solution

Traditional methods of orthogonal mode shapes cannot be applied here due to the nonself-adjoint operator. However, by extending the problem definition onto a virtual duct, and then redefining the eigenfunctions over  $[-L, L]$ , the time and space modes will decouple and a solution to the problem can be found. This technique is explained below.

The solution to the forced wave equation is now written as a series solution plus a time dependent term arising from the  $\lambda=0$  eigenvalue



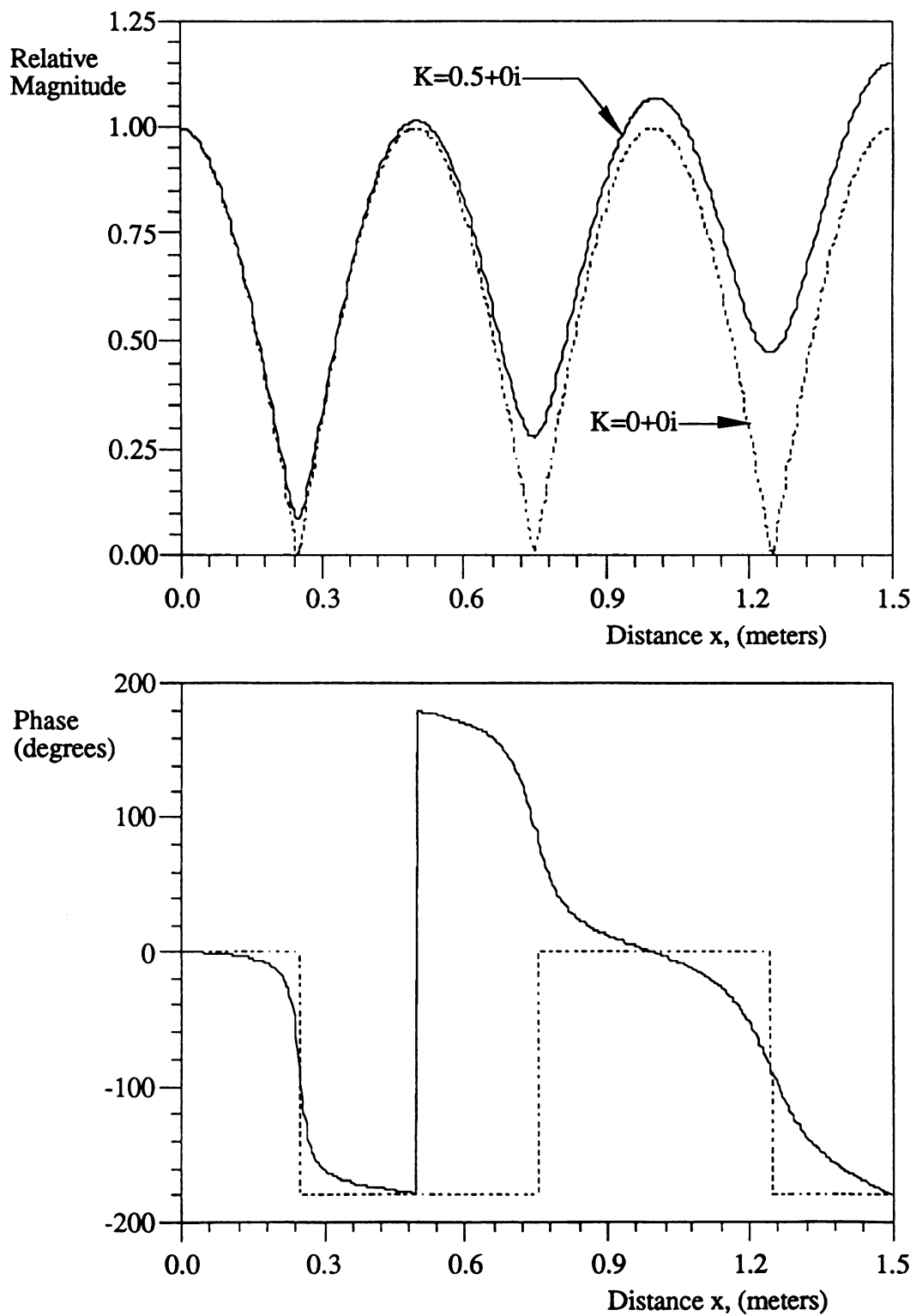


Figure 2.1. Third Eigenfunction for Duct Particle Displacement with End Impedances:  $K = 0.5+0i$  and  $K = 0+0i$ .

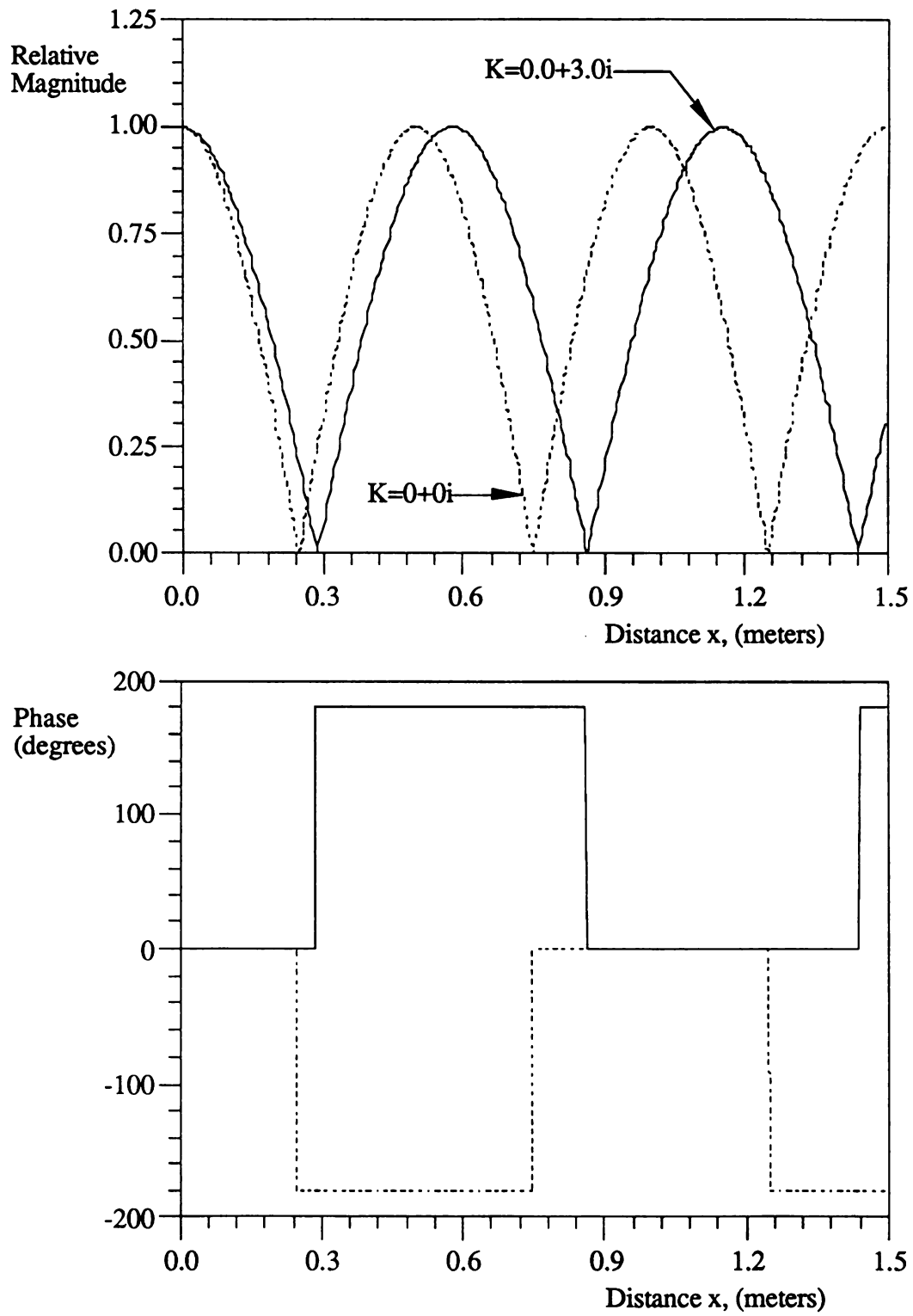


Figure 2.2. Third Eigenfunction for Duct Particle Displacement with End Impedances:  $K = 0+0i$  and  $K = 0.0+3.0i$ .

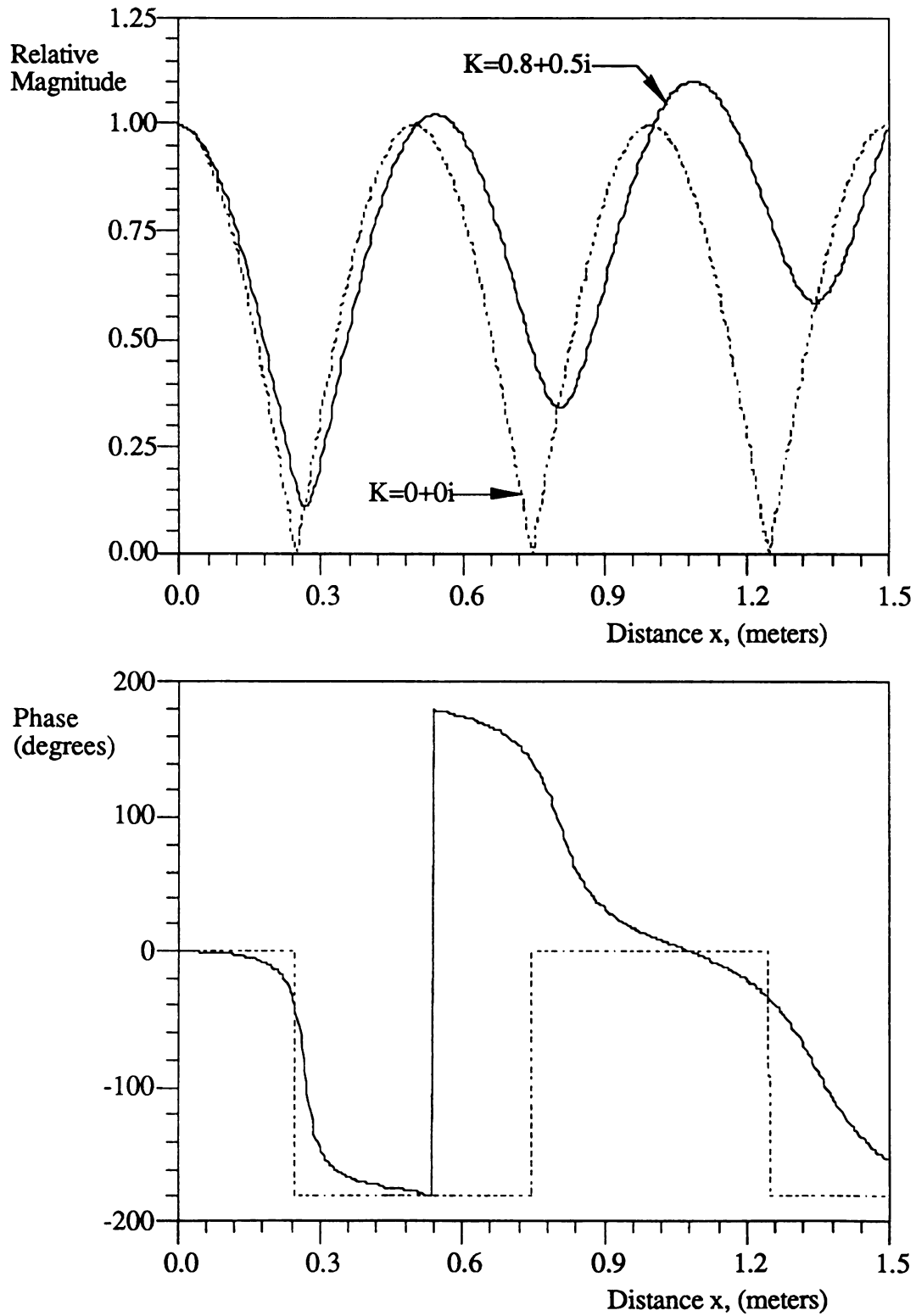


Figure 2.3. Third Eigenfunction for Duct Particle Displacement with End Impedances:  $K = 0+0i$  and  $K = 0.8+0.3i$ .



$$u(x,t) = G(t) + \sum_{n=-\infty}^{+\infty} a_n(t) \phi_n(x) \quad (2.12)$$

where  $G(t)$  and  $a_n(t)$  are state variables (generalized coordinates) and  $\phi_n(x)$  are the eigenfunctions defined in (2.11). The coordinate  $G(t)$  will not contribute to the pressure response in the duct because the pressure response is only dependent on the spatial partial derivative. To derive the state space representation, the time derivative of the wave equation is expressed in two different forms. The first uses (2.12) giving

$$\frac{\partial u}{\partial t}(x,t) = \dot{G}(t) + \sum_{n=-\infty}^{+\infty} \dot{a}_n(t) \phi_n(x) \quad (2.13)$$

The second arises using (2.5) and (2.9) as

$$\frac{\partial u}{\partial t}(x,t) = \sum_{n=-\infty}^{+\infty} c\lambda_n a_n(t) \phi_n(x) \quad (2.14)$$

Equating (2.13) and (2.14) results in

$$\dot{G}(t) + \sum_{n=-\infty}^{+\infty} [\dot{a}_n(t) - c\lambda_n a_n(t)] \phi_n(x) = 0 \quad (2.15)$$

The assumption is now made that the differentiation will distribute over the summation. Success with decoupling will validate this assumption. Evaluating the forced wave equation (2.1) by inserting the second spatial derivative of (2.12) and the first time derivative of (2.14) produces

$$\sum_{n=-\infty}^{+\infty} [\dot{a}_n(t) - c\lambda_n a_n(t)] c\lambda_n \phi_n(x) = -\frac{\partial}{\partial x} \left[ \frac{\delta(x) P(t)}{\rho} \right] - \sum_{i=1}^k [\delta(x - x_i)] \frac{\partial}{\partial t} \left[ \frac{M_i(t)}{\rho S} \right] \quad (2.16)$$

## 2.5. A New Inner Product

Independent ordinary differential equations for each generalized coordinate  $a_n(t)$  are found by differentiating (2.15) with respect to the spatial variable  $x$  and multiplying by  $c$ . The result is then added to equation (2.16) to form

$$\sum_{n=-\infty}^{+\infty} [\dot{a}_n(t) - c\lambda_n a_n(t)] 2c\lambda_n e^{\lambda_n x} = -\frac{\partial}{\partial x} \left[ \frac{\delta(x)P(t)}{\rho} \right] - \sum_{i=1}^k [\delta(x - x_i)] \frac{\partial}{\partial t} \left[ \frac{M_i(t)}{\rho S} \right]$$

$x \in [0, L]$  (2.17)

and subtracted from equation (2.16) to yield

$$\sum_{n=-\infty}^{+\infty} [\dot{a}_n(t) - c\lambda_n a_n(t)] 2c\lambda_n e^{-\lambda_n x} = -\frac{\partial}{\partial x} \left[ \frac{\delta(x)P(t)}{\rho} \right] - \sum_{i=1}^k [\delta(x - x_i)] \frac{\partial}{\partial t} \left[ \frac{M_i(t)}{\rho S} \right]$$

$x \in [0, L]$  (2.18)

respectively. The interval of (2.18) is then changed to  $[-L, 0]$  by substitution of  $-x$  for  $x$  yielding

$$\sum_{n=-\infty}^{+\infty} [\dot{a}_n(t) - c\lambda_n a_n(t)] 2c\lambda_n e^{\lambda_n x} = -\frac{\partial}{\partial x} \left[ \frac{\delta(-x)P(t)}{\rho} \right] + \sum_{i=1}^k [\delta(-x - x_i)] \frac{\partial}{\partial t} \left[ \frac{M_i(t)}{\rho S} \right]$$

$x \in [-L, 0]$ . (2.19)

To guarantee the same effect over  $[-L, 0]$  as  $[0, L]$  the mass flow input term  $[\delta(x - x_i)] \partial M_i(t) / \partial t$  must be extended as an odd function on  $[-L, L]$  because it interacts with an odd local pressure. For this reason, it undergoes a sign change in (2.19). The pressure gradient  $\partial[\delta(x)P(t)] / \partial x$  is an even function for the above mentioned reason, so the sign remains unchanged. Combining (2.17) and (2.19) using (2.10) and breaking the exponential into terms that contain the index  $n$  and terms that do not contain the index  $n$  results in

$$\sum_{n=-\infty}^{+\infty} [\dot{a}_n(t) - c\lambda_n a_n(t)] 2c\lambda_n e^{\frac{-in\pi x}{L}} =$$

$$\begin{cases} e^{\left(\frac{-1}{2L} \log_e \frac{1-K}{1+K}\right)x} \left[ -\frac{\partial}{\partial x} \left[ \frac{\delta(-x)P(t)}{\rho} \right] + \sum_{i=1}^k [\delta(-x-x_i)] \frac{\partial}{\partial t} \left[ \frac{M_i(t)}{\rho S} \right] \right] & x \in [-L, 0] \\ e^{\left(\frac{-1}{2L} \log_e \frac{1-K}{1+K}\right)x} \left[ -\frac{\partial}{\partial x} \left[ \frac{\delta(x)P(t)}{\rho} \right] - \sum_{i=1}^k [\delta(x-x_i)] \frac{\partial}{\partial t} \left[ \frac{M_i(t)}{\rho S} \right] \right] & x \in [0, L]. \end{cases} \quad (2.20)$$

An exponential  $e^{im\pi x/L}$  is now multiplied on both sides of (2.20) and the resulting equation is integrated from  $-L$  to  $L$ . The functions on the left hand side of the integral equation are orthogonal and have a nonzero value only when indices  $n=m$  giving

$$\int_{-L}^L [\dot{a}_{nm}(t) - c\lambda_n a_{nm}(t)] 2c\lambda_n e^{\frac{-in\pi x}{L}} e^{\frac{im\pi x}{L}} dx =$$

$$\begin{cases} [\dot{a}_{nm}(t) - c\lambda_n a_{nm}(t)] 4c\lambda_n L & n = m \\ 0 & n \neq m \end{cases} \quad (2.21a)$$

Using the reflection property of integrals, the right hand side of (2.20) becomes

$$\int_{-L}^0 e^{\frac{im\pi x}{L}} e^{\left(\frac{-1}{2L} \log_e \frac{1-K}{1+K}\right)x} \left[ -\frac{\partial}{\partial x} \left[ \frac{\delta(-x)P(t)}{\rho} \right] + \sum_{i=1}^k [\delta(-x-x_i)] \frac{\partial}{\partial t} \left[ \frac{M_i(t)}{\rho S} \right] \right] dx +$$

$$\int_0^L e^{\frac{im\pi x}{L}} e^{\left(\frac{-1}{2L} \log_e \frac{1-K}{1+K}\right)x} \left[ -\frac{\partial}{\partial x} \left[ \frac{\delta(x)P(t)}{\rho} \right] - \sum_{i=1}^k [\delta(x-x_i)] \frac{\partial}{\partial t} \left[ \frac{M_i(t)}{\rho S} \right] \right] dx =$$

$$\frac{-2P(t)}{\rho} + \sum_{i=1}^k \frac{\partial}{\partial t} \left[ \frac{M_i(t)}{\rho S} \right] \left( \frac{1}{\lambda_n} \right) \frac{d\phi_n(x_i)}{dx} \quad (2.21b)$$

Equations (2.21a) and (2.21b) can be equated to form

$$[\dot{a}_n(t) - c\lambda_n a_n] = \frac{-P(t)}{2c\lambda_n L\rho} + \sum_{i=1}^k \frac{\partial}{\partial t} \left[ \frac{M_i(t)}{4c\lambda_n^2 L\rho S} \right] \frac{d\phi_n(x_i)}{dx} \quad (2.22)$$

This is the ordinary differential equation for each of the state variables  $a_n(t)$ .

## 2.6. State Space Formulation

The infinite order state space formulation is taken directly from (2.22) which is rewritten in matrix form as

$$\dot{\mathbf{a}}(t) = \mathbf{A}\mathbf{a}(t) + \mathbf{B}\mathbf{m}(t) + \mathbf{b}_p p(t) \quad (2.23)$$

where  $\mathbf{a}(t)$  = the vector of modal wave amplitudes  $a_n(t)$ ,

$\mathbf{A}$  = the diagonal matrix  $[c\lambda_n]$ ,

$\mathbf{B}$  = the matrix  $\left\{ \left[ \frac{1}{4c\lambda_n^2 L\rho S} \right] \frac{d\phi_n(x_i)}{dx} \right\}$ ,

$\mathbf{m}(t)$  = the vector of mass flow inputs  $\partial[M_1, \dots, M_k]^T / \partial t$ ,

$\mathbf{b}_p$  = the vector  $\left[ \frac{-1}{2c\lambda_n L\rho} \right]$ , and

$p(t)$  = the pressure input at  $x = 0$ ,

$$P(x_m, t) = \mathbf{c}^T \mathbf{a}(t), \quad (2.24)$$

where  $P(x_m, t)$  = the pressure in the duct at  $x = x_m$ ,

and  $\mathbf{c}$  = the vector  $[-\rho c^2 \frac{d\phi_n(x_m)}{dx}]$ .

$\mathbf{A}$  is diagonal because the result of the inner product (2.21) is nonzero only when  $n=m$  along the diagonal. The resulting state space representation is extremely useful since the individual modes are decoupled from each other and each state's input from each excitation is explicit.



The initial conditions on the  $a_n(t)$  coordinates are found using a similar method to the derivation (2.12) - (2.22), which produces

$$a_n(0) = \frac{1}{4L\lambda_n c} \int_0^L \frac{\partial u}{\partial t}(x,0) \varphi_n(x) dx - \frac{1}{4L\lambda_n^2} \int_0^L \frac{\partial u}{\partial x}(x,0) \frac{d\varphi_n(x)}{dx} dx \quad . \quad (2.25)$$

## 2.7. Frequency Response

The general form of the transient time response to harmonic pressure excitation at  $x=0$  is found by solving for each of the states  $a_n(t)$  as

$$a_n(t) = \left[ a_n(0) - \frac{d_n}{i\omega - c\lambda_n} \right] e^{c\lambda_n t} + \frac{d_n}{i\omega - c\lambda_n} e^{i\omega t} \quad (2.26)$$

$$\text{with } d_n = \frac{P_0}{2c\lambda_n L \rho} \quad \text{and } P(t) = -P_0 e^{i\omega t}.$$

The steady state response of (2.26) is

$$\tilde{a}_n(t) = \frac{P_0 e^{i\omega t}}{2c\lambda_n L \rho (i\omega - c\lambda_n)} \quad . \quad (2.27)$$

Finally inserting the  $a_n(t)$  back into the original series solution and using (2.4) to evaluate the pressure response produces the following series solution

$$P(x,t) = -\rho c^2 \sum_{n=-\infty}^{+\infty} \tilde{a}_n(t) \frac{d\varphi_n(x)}{dx} \quad . \quad (2.28)$$

Evaluating (2.28) with a finite number of symmetric terms yields the following truncated series solution

$$P_N(x,t) = -\rho c^2 \sum_{n=-N}^{+N} \tilde{a}_n(t) \frac{d\varphi_n(x)}{dx} \quad . \quad (2.29)$$



## 2.8. Accuracy of Truncated Solution

The exact, infinite-order transient response to this duct problem has not been previously available. The exact series form for the transient solution for pressure excitation and/or mass flow excitation must be truncated to a finite number of terms for engineering use. The effect of this truncation on both steady state and transient forms of the exact series solution will now be examined. The effect of truncation on a control system using a truncated model is to introduce observation and control spillover which occurs whenever an unmodeled mode in the system interacts with the control system action. This spillover typically degrades performance and in extreme cases lead to closed-loop control system instability.

Quantitative information on the accuracy of a truncated, steady state, series solution (2.29) is found here by comparing it to an exact, steady state, frequency response. The exact steady state response for the system described in (2.1-2.3) can be independently calculated (Spiekermann, 1986; Spiekermann and Radcliffe, 1988) for the special case of harmonic pressure excitation only with a closed form solution (2.29) as

$$P(x,t) = P_0 \left[ \frac{(K-1)e^{i\frac{\omega}{c}(x-L)} + (K+1)e^{-i\frac{\omega}{c}(x-L)}}{(K-1)e^{-i\frac{\omega}{c}x} + (K+1)e^{i\frac{\omega}{c}x}} \right] e^{i\omega t} \quad (2.30)$$

This exact steady state response model is only valid for the special case of pressure excitation at  $x=0$ . It can not model the mass flow excitation in the domain nor does it model transient responses. It is used here only for comparison with the more general result (2.28).

Figure 2.4 is a frequency response of a 1.524 m (5 ft) duct at location  $x=0.4267$  m (1.4 ft) from the pressure excitation at  $x=0$ . The impedance is  $K=0.3+0.2i$  and a truncated series model with eleven terms is used to approximate the solution. The solid line is the



truncated steady state series solution (2.29) and the dotted line is the exact solution (2.28, 2.30). The mean relative error up to the fifth duct resonance is 3.2% (-30 dB). Numerical simulations suggest the state space model requires one state to model zero frequency response plus two states per duct resonance. The model yields acceptable accuracy up to the highest duct resonance modeled.

The error of the truncated solution to this acoustic problem is periodic and bounded. This situation can be demonstrated (Figure 2.5) with the eleven term model (Figure 2.4). This is unlike typical mechanical systems (Chait et al., 1988) that have a vanishing bound as the forcing frequency approaches infinity. The impact on a control system is that the higher frequency modal magnitudes are not small and cannot be ignored. The truncated state space solution for system frequency response approaches zero as the driving frequency approaches infinity. The state space solution is exponentially stable (Kwakernaak and Sivan, 1972). Exponential stability is guaranteed since the real parts of all the eigenvalues are negative and  $\mathbf{B}$  and  $\mathbf{b}$  are bounded.

Figure 2.6 is a frequency response of a 1.524 m duct at location  $x=0.4267$  m from the end. In this example, the excitation has been moved from  $x=0$  to  $x_i=1.22$  m (4 ft) where it is now a mass flow excitation. The mass flow excitation term is  $M(t) = -M_0 e^{i\omega t}$ . The impedance is  $K=0.3+0.2i$  and fifteen terms are used to form the solution. The previous steady state model (2.30) cannot be compared to this frequency response since it is only valid for pressure excitation at  $x=0$  and frequency  $\omega$ . The resonance peaks still occur at the same frequency as (2.30). This is predicted behavior since the modes are not dependent on excitation location.

## 2.9. Transient Response

The solution to a transient problem is shown in Figure 2.7. The input into the duct is a harmonic pressure excitation with a frequency of 150 Hertz initiated at  $t=0$ . The input location is  $x=0$  and the response is calculated at location  $x=0.914$  (3 ft). The solid line is the five term solution and the dotted line is a 51 term solution. The impedance constant is  $K=0.3+0.2i$ . The duct acoustic pressure and particle velocity are zero at time  $t=0$  yielding zero initial conditions for all model states. Since the state model is diagonal, the response of the generalized coordinates (states) are independent. Adding additional terms to the state model does not alter the response of each of the previous states. This behavior does not occur for coupled state space models with nondiagonal  $A$  matrices. Because the states are decoupled, modal truncation error is reduced and predicted response with only 5 terms is quite similar to that for 51 terms.

The solution to another transient problem is shown in Figure 2.8. The input into the duct is a pressure pulse of magnitude one and width of 0.001 seconds. The input location is  $x=0$  and the response is calculated at location  $x=0.610$  m (2 ft). The impedance constant is  $K=0.3+0i$ . The solid line is the 51 term solution which approximates the exact solution very well and the dashed line is the 11 term solution which has the same response in each of the states but lower resolution due to the reduction in state number. The exact solution pulse magnitude which can be calculated for this simple special case equals one for the first pulse. Every successive pulse then decreases by 54.8% due to energy escaping from the end of the duct. The exact solution pulse width is 0.001 seconds and the first one occurs at  $t=0.00183$  seconds. The truncated series solution has these characteristics. Because the forcing function is a pulse with infinite Fourier series, adding additional states in this example helps the accuracy of the solution.

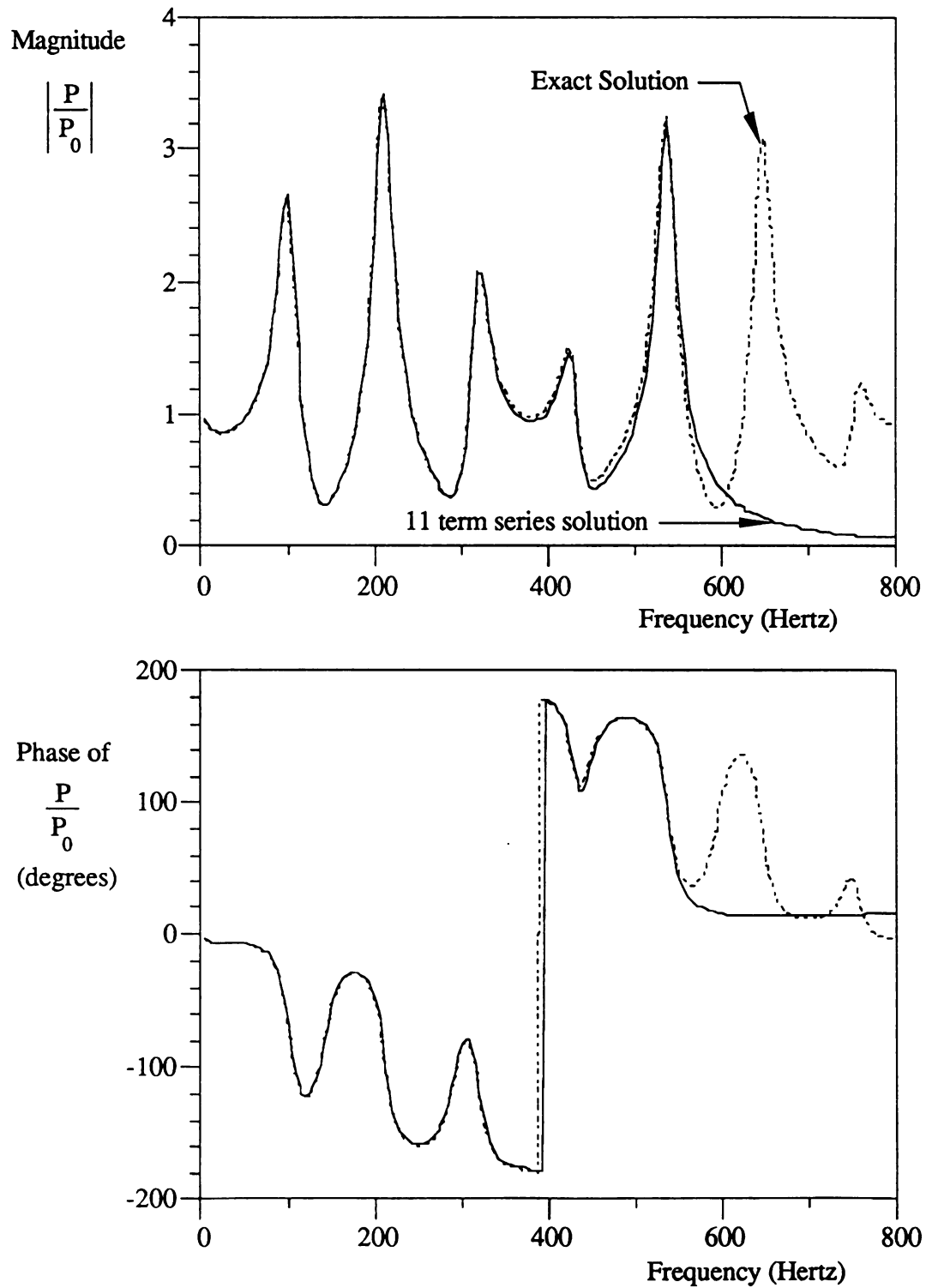


Figure 2.4. End-Point ( $x=0$ ) Pressure Excited Steady State Frequency Response with an Impedance Constant of  $K = 0.3+0.2i$  at  $x = 0.4267$  m.

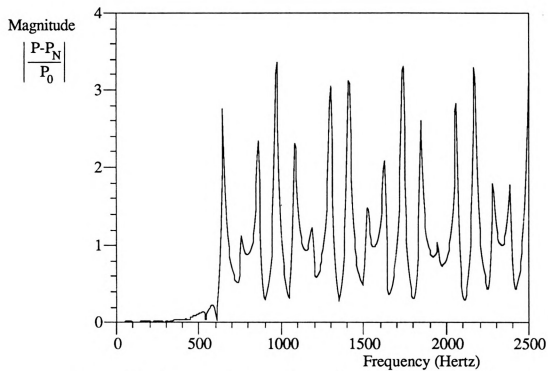


Figure 2.5. Frequency Response Truncation Error of an 11 Term Model with Impedance Constant of  $K = 0.3 + 0.2i$ .



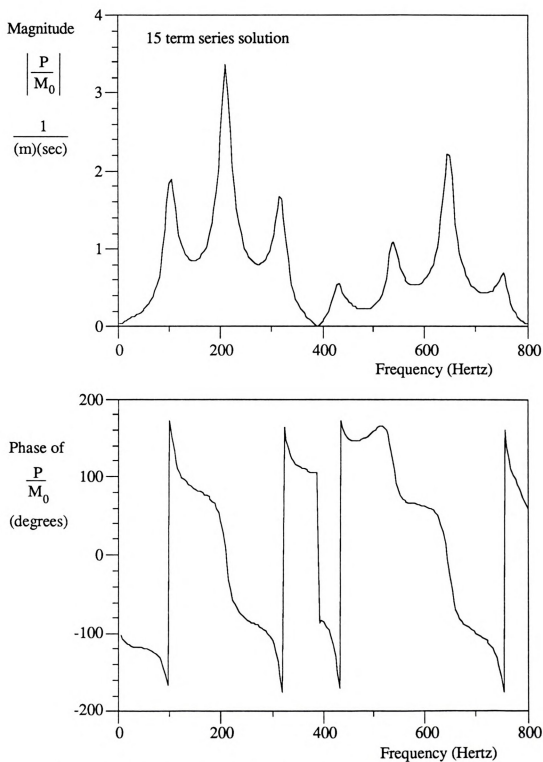


Figure 2.6. Interior Point Mass Flow Excited Steady State Frequency Response with an Impedance Constant of  $K = 0.3 + 0.2i$  at  $x = 0.4267$  m. Excitation at  $x_1 = 1.22$  m.

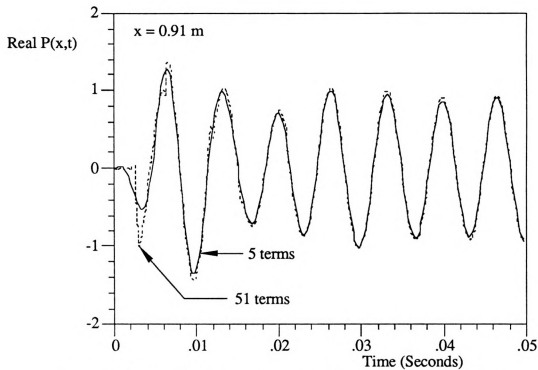


Figure 2.7. Harmonic Time Response of 5 and 51 Term Duct Models with an Impedance Constant of  $K = 0.3 + 0.2i$ .

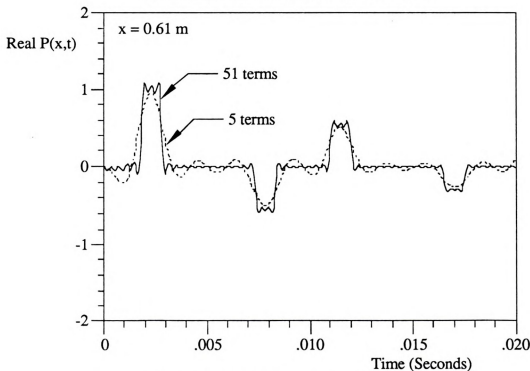


Figure 2.8. Pulse Time Response of a 1.5 m Duct with an End Impedance of  $K = 0.3 + 0i$ .



## Chapter 3. Experimental Verification of the State Space Model\*

### 3.1. Model Verification Experiment

The state space model developed in Chapter 2 is experimentally verified for four different test cases. Open loop verification of the model is essential if real time control is to be successfully applied to the duct. In all the experiments, the impedance at the end of the duct was calculated from the experimental system transfer functions. This measurement technique is discussed in Chapter 4.

### 3.2. Pressure Excitation, Constant Acoustic Impedance

The first experiment involved pressure excitation at  $x=0$  with a constant, frequency invariant, acoustic impedance in the termination end. The impedance was produced by inserting a flat piece of packing foam which had a nearly constant impedance at all frequencies of interest. The steady state response of (2.23) to harmonic excitation using the pressure excitation term is

$$a_n(t) = \frac{P_0 e^{i\omega t}}{2c\lambda_n L \rho(i\omega - c\lambda_n)} \quad (3.1)$$

where the pressure is evaluated using (2.4), (2.5) and (2.11). The experiment used a 76 mm (3 in) circular PVC schedule 40 duct that was 2.60 m (8.52 ft) long driven by a 254 mm (10 in) diameter speaker (Realistic 40-1331B). Speaker input pressure was measured in the exit plane of the input speaker with a Bruel and Kjaer Type 4166 half inch

---

\* This chapter is based on the paper "Experimental Verification of the Nonself-Adjoint State Space Duct Model," submitted for publication to the *ASME Journal of Vibration and Acoustics*.

microphone attached to a Hewlett Packard 5423A digital signal analyzer. At a location of  $x=0.792$  m (2.60 ft) from the speaker, the response of the tube was measured with another Bruel and Kjaer Type 4166 half inch microphone. The output of the response microphone was then connected to the signal analyzer (Figure 3.1). Both microphones were calibrated using a Bruel and Kjaer Type 4230 Sound Level Calibrator. The packing foam had a measured acoustic impedance of approximately  $K=0.285+0.079i$  from zero to 400 Hertz.

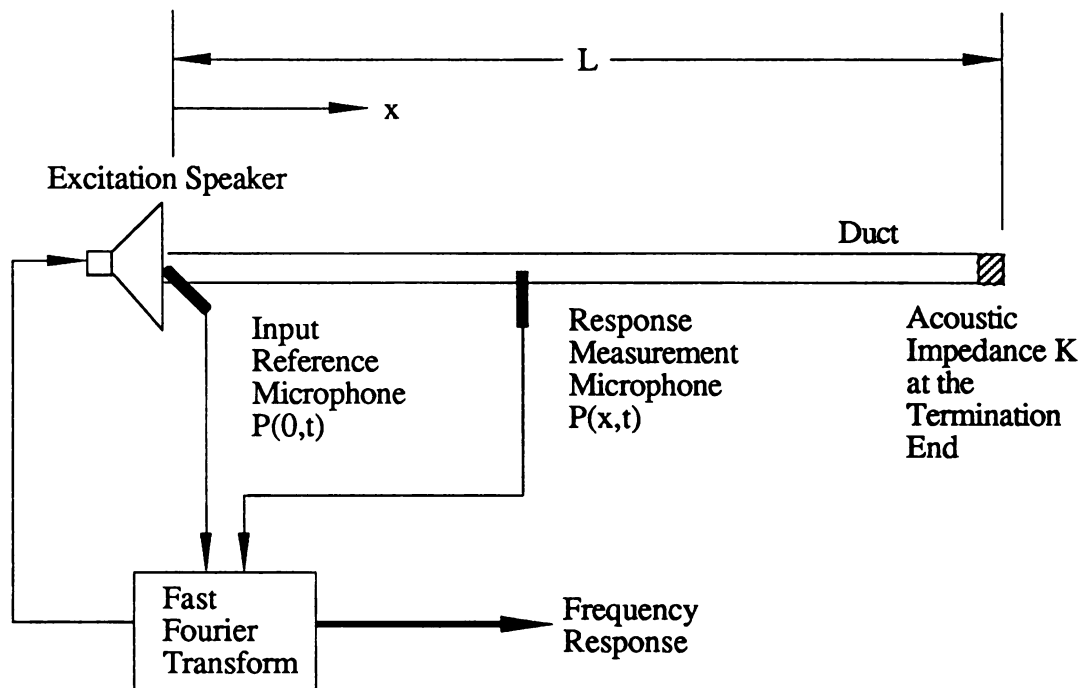


Figure 3.1. Laboratory Configuration.

The results of the experiment are shown in Figure 3.2. The measured responses are marked by X's and the theoretical response with the measured end impedance is denoted by a solid line. There is a high degree of accuracy in the magnitude and the phase data. The disagreement between the experimental data and the theory are possibly due to a slight nonlinearity of the packing foam impedance.

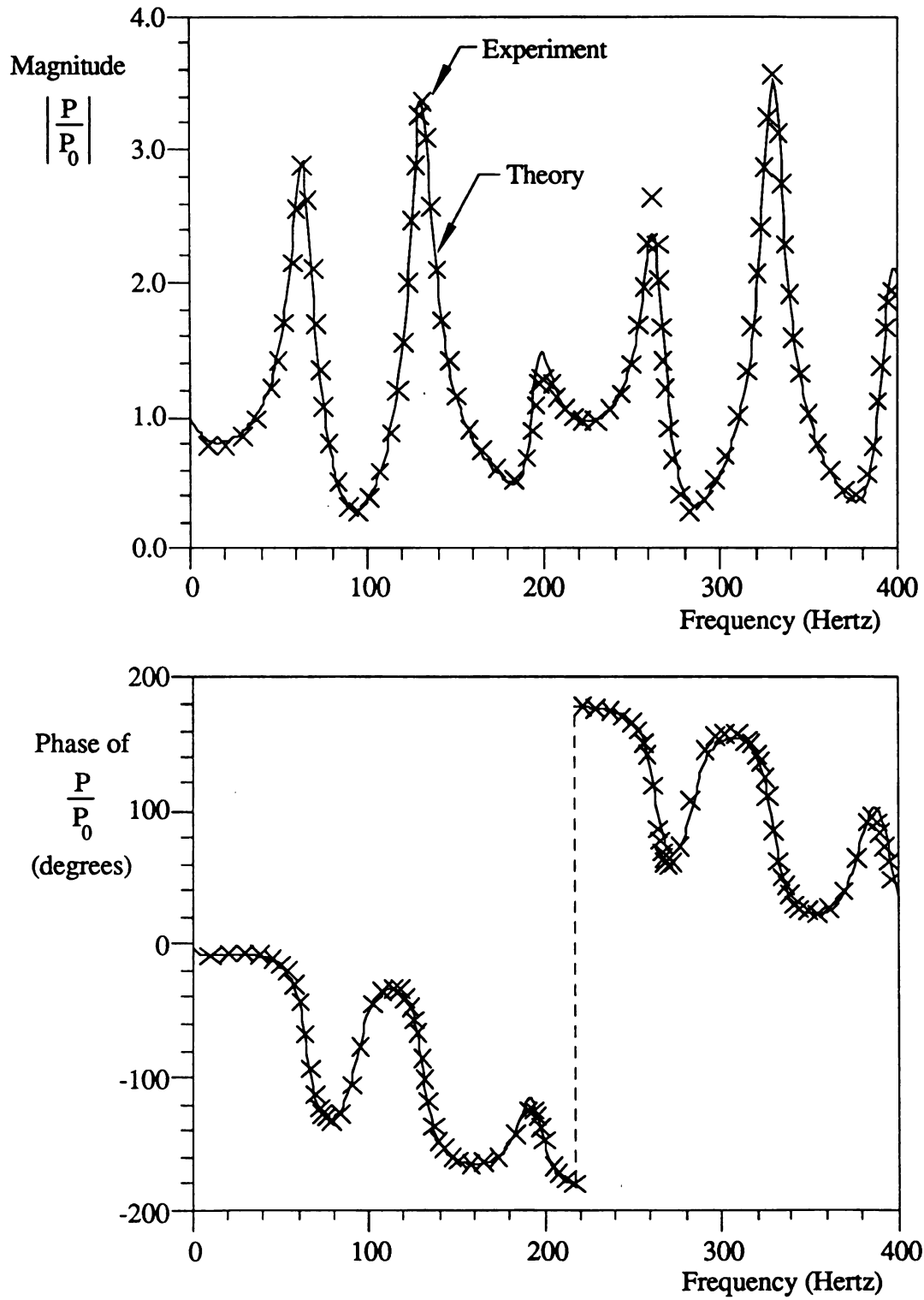


Figure 3.2. Frequency Response of Duct with End Pressure Excitation.



### 3.3. Mass Flow Excitation, Constant Acoustic Impedance

The experiment was rerun with mass flow excitation in the domain. The steady state response of (2.23) for mass flow excitation is

$$a_n(t) = \frac{-M_0 e^{i\omega t}}{4c\lambda_n^2 L \rho S(i\omega - c\lambda_n)} \left[ \frac{d\phi_n(x_i)}{dx} \right] \quad (3.2)$$

where the pressure is evaluated using the same equations as in experiment 1. A Realistic 102 mm (4 in) speaker was located in the wall of the duct at  $x_1=1.58$  m (5.17 ft) using a schedule 40 test tee. The input signal was measured using a Bruel and Kjaer Type 3544 helium neon laser velocity measurement system attached to the signal analyzer. The laser measured the velocity of the speaker cone which is proportional to the mass flow. The test tee had a plexiglass window inserted in its side so the laser could shine on the speaker cone face to measure its velocity. The length of the duct tested was 4.42 m (14.5 ft) and the response was measured at  $x=0.762$  m (2.50 ft). The foam used in the first experiment was again used in this experiment. The results of the experiment are shown in Figure 3.3.

### 3.4. Pressure Excitation, Nonconstant Acoustic Impedance

The acoustic impedance of the systems discussed here is given in (2.2). Equation (2.2) makes the assumption that the acoustic impedance is constant. For some termination ends, the impedance is frequency dependent. For these systems, (2.2) is written as

$$\frac{\partial u}{\partial x}(L, t) = -K(\omega) \left( \frac{1}{c} \right) \frac{\partial u}{\partial t}(L, t) \quad K \neq 0+0i, 1+0i, \infty \quad (3.3)$$

Although the separation of variables in Chapter 2 is for  $K$  constant, termination ends where  $K$  is a function of frequency can be approximated by

$$\left. \frac{\partial u}{\partial x}(L, t) \right|_{\omega=\omega_n} = -K_n \left( \frac{1}{c} \right) \left. \frac{\partial u}{\partial t}(L, t) \right|_{\omega=\omega_n} \quad K \neq 0+0i, 1+0i, \infty, \quad n = 0, 1, 2, \dots \quad (3.4)$$



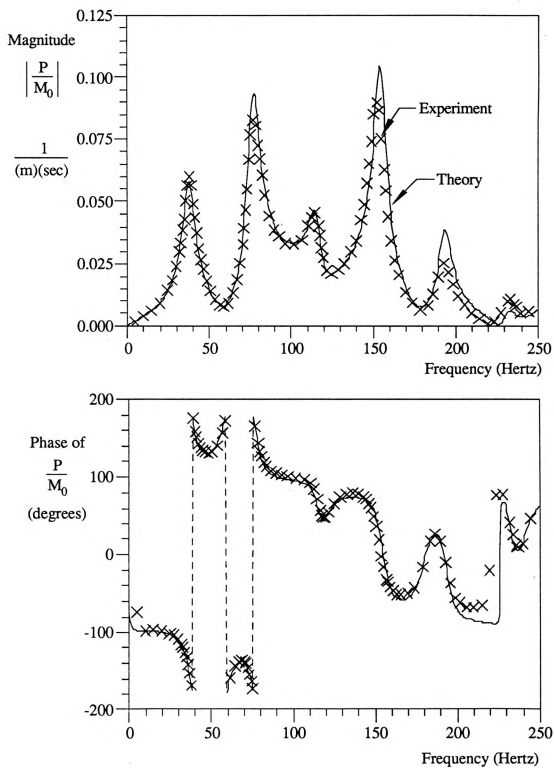


Figure 3.3. Frequency Response of Duct with Interior Mass Flow Excitation.



Using this relationship, the state space model derived in Chapter 2 can be used to approximate systems with frequency dependent terminations. An example is given below.

The third experiment involved pressure excitation at  $x=0$  with a nonconstant acoustic impedance in the termination end. The nonconstant termination was produced by placing a hemisphere of foam with a diameter equal to the duct's diameter in the end of the duct. The resulting acoustic wave was effected by the foam material as well as the shape of the material. This produced a nonconstant acoustic impedance. The values are listed in Table 3.1. They were found by obtaining a frequency response of the system from zero to 800 Hertz and then solving the inverse problem for  $K$  at each duct eigenvalue (Chapter 3). The length of the duct was 1.59 m (5.22 ft) and the response was measured at  $x=1.09$  m (3.56 ft). The state space model was then assembled using the individual acoustic impedance measurements of  $K$  at each resonant frequency rather than a single value for  $K$ . The eigenvalues of the system are non-conjugate complex values since  $K$  is complex. The results are shown in Figure 3.4. Figure 3.4 demonstrates that for a nonconstant impedance end the linear state space model is reasonably accurate and can predict resonant peak locations as well as system phase angles. The errors tend to be minimized near the natural frequencies and maximized between the natural frequencies. This is because the modal impedances,  $K_n$ , were measured at the natural frequencies. The model does not account for varying values of the impedance between the modes.



Table 3.1. Calculated Acoustic Impedance.

Eigenvalue (n)	$\omega_n$ (Hertz)	Re ( $K_n$ )	Im ( $K_n$ )
1	104.8	0.599	0.066
2	213.8	0.585	0.054
3	314.6	0.594	0.206
4	424.2	0.522	0.198
5	533.5	0.491	0.182
6	645.0	0.508	0.104
7	754.6	0.459	0.081



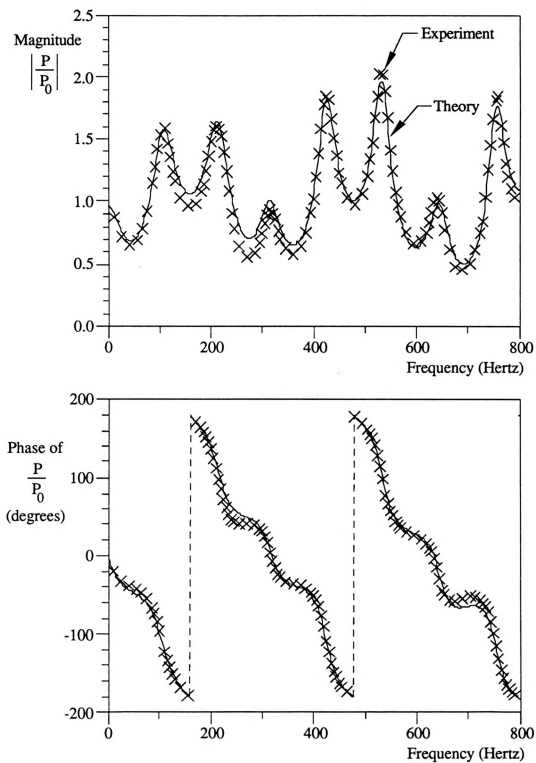


Figure 3.4. Frequency Response of Duct with Nonconstant Acoustic Impedance.

### 3.5. Transient Response

The pressure excitation steady-state responses presented previously can be computed from previous steady-state solutions (Davis et al., 1954, Spiekermann, 1986) to the wave equation as well as the state space model investigated here. The general transient response to pressure and flow excitation has not been available previously and the transient response of a state model is required to implement modern control methods. This transient response was verified in the set of experiments below.

The experiment was initiated by attaching a signal generator to the excitation speaker and caused one cycle of sine wave excitation at approximately 500 Hertz (Figure 3.5). The system input pressure and response pressure were then measured by Bruel and Kjaer Type 4166 half inch microphones attached to an Apple Computer, Inc. Macintosh IIX computer running National Instruments Labview software and an NB-MIO-16L analog to digital converter. The measured time domain experimental data was then compared to theoretical model response. The length of the duct in this test was 2.44 m (8.00 ft) and the response was measured at  $x=0.792$  m (2.60 ft). The packing foam used in the first experiment was also used in this experiment to provide a nonzero acoustic impedance in the end of the duct.

Figure 3.6 is a plot of the experimental data and theoretical state space model. The solid line is the experimental data and the dashed line is the theoretical model. The theoretical model response was computed using a fifth order Adams' integration method with 51 states. The forcing function in the Adams' integration routine was the measured system input at  $x=0$ . The integration step size was  $\Delta t=0.000035$  which matched the Labview sampling rate of 28571 Hertz. There is an excellent match between the theoretical model and experimental data from  $t=0$  to  $t=0.015$  seconds. After that, the experimental data and theoretical prediction deviate because the propagating pressure pulse reflects off the now inactive speaker and is effected by the speakers impedance. The theoretical model



does not account for impedance at the speaker, however, Figures 3.1 and 3.3 illustrate that an active speaker has little effect on the impedance at the source end.

Truncation effects of the state space model are shown in Figures 3.7 and 3.8. Figure 3.7 is the experimental data compared to a 21 term state space model and Figure 3.8 is the experimental data compared to a 15 term state space model. The 51 term state space model has an error at the pulse peak of less than 1% that increases to an error of 15% for the 21 term state space model and further increases to 40% for the 15 term state space model. Models with less than 15 terms do not have the bandwidth required to give a reasonable solution accuracy for the approximately 500 Hertz transient input used in this experiment. In general, more terms used in the model produces a more accurate solution because the model bandwidth is increased with the addition of each mode. Most real-time control schemes cannot incorporate a large number of model terms due to the speed required to control the system. There is always a trade off between control complexity (model size) and bandwidth (speed of response) in any control system. These issues are especially important in distributed parameter control systems (Chait et al., 1988).

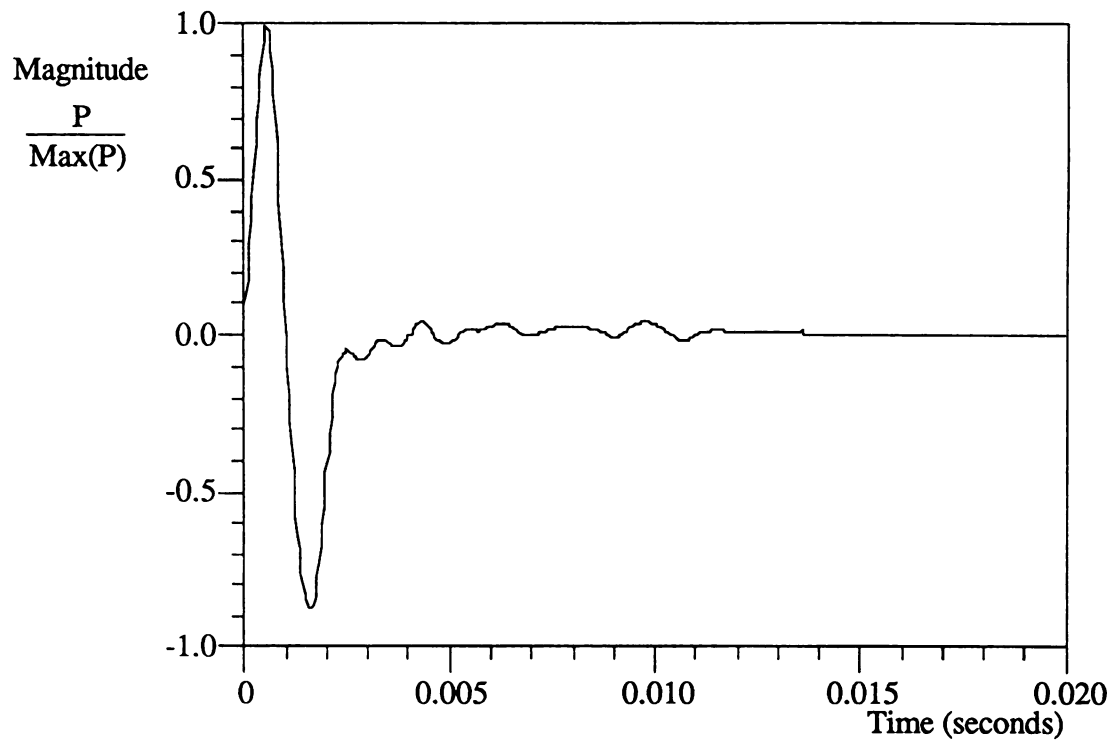


Figure 3.5. System Pressure Input at  $x=0$ .

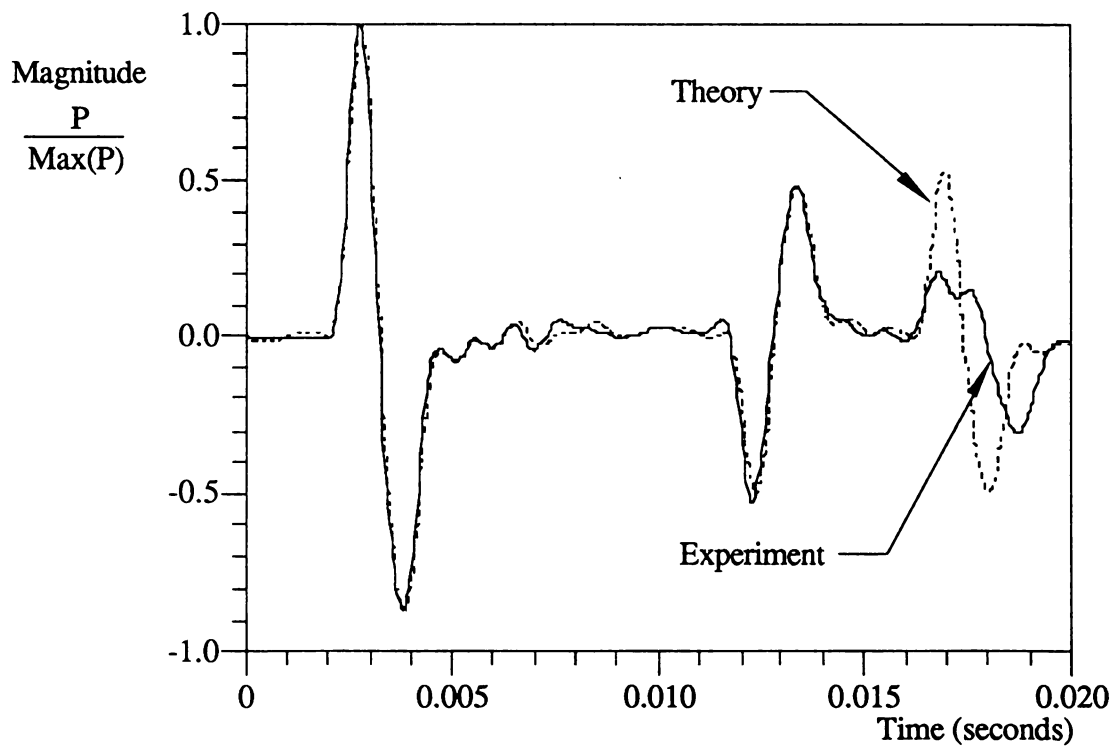


Figure 3.6. Transient Response of Duct at  $x=0.792$  m with 51 Term Model.

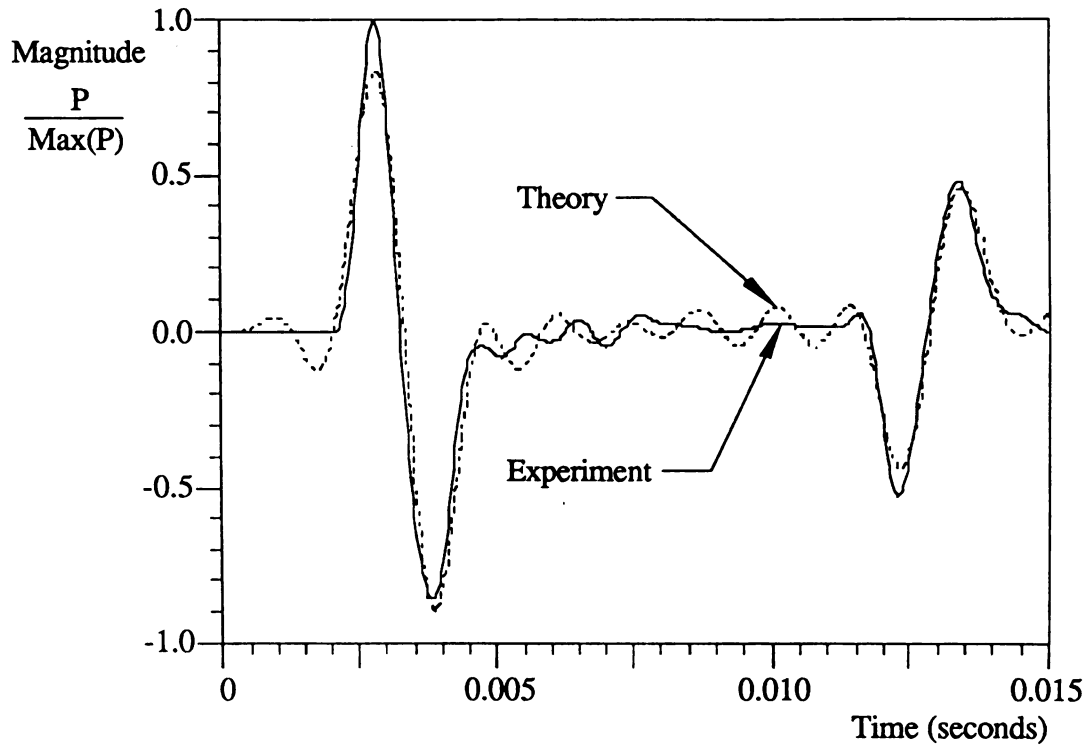


Figure 3.7. Transient Response of Duct with 21 Terms.

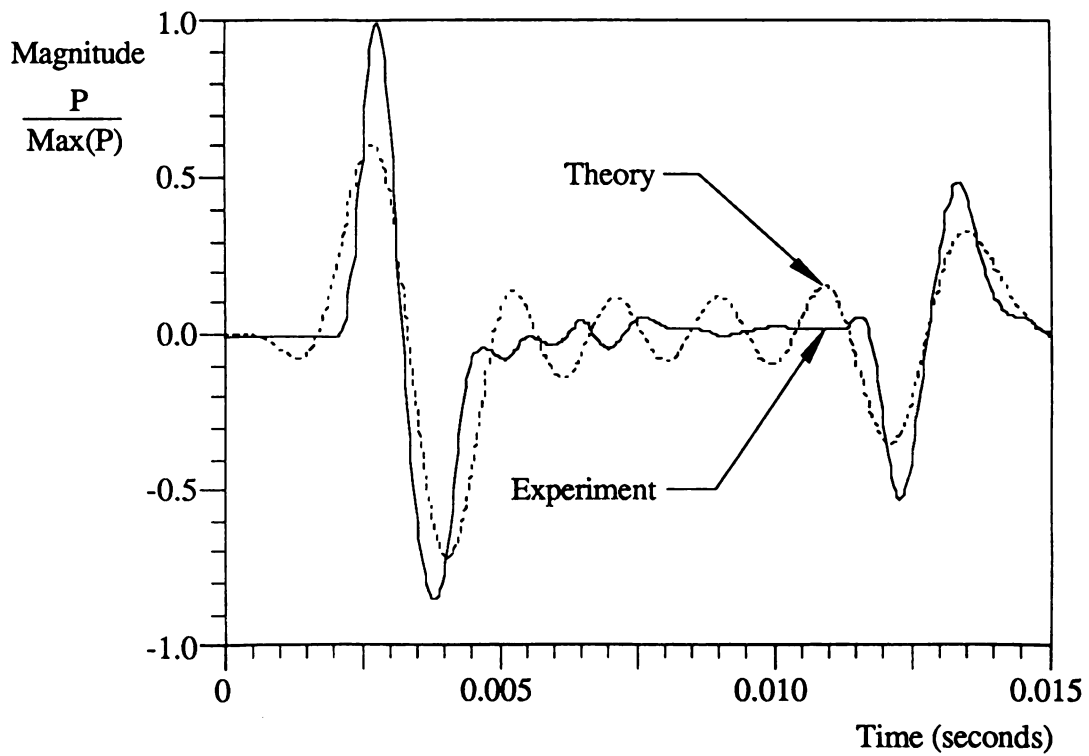


Figure 3.8. Transient Response of Duct with 15 Terms.



## Chapter 4. Acoustic Impedance Measurement\*

### 4.1. Introduction

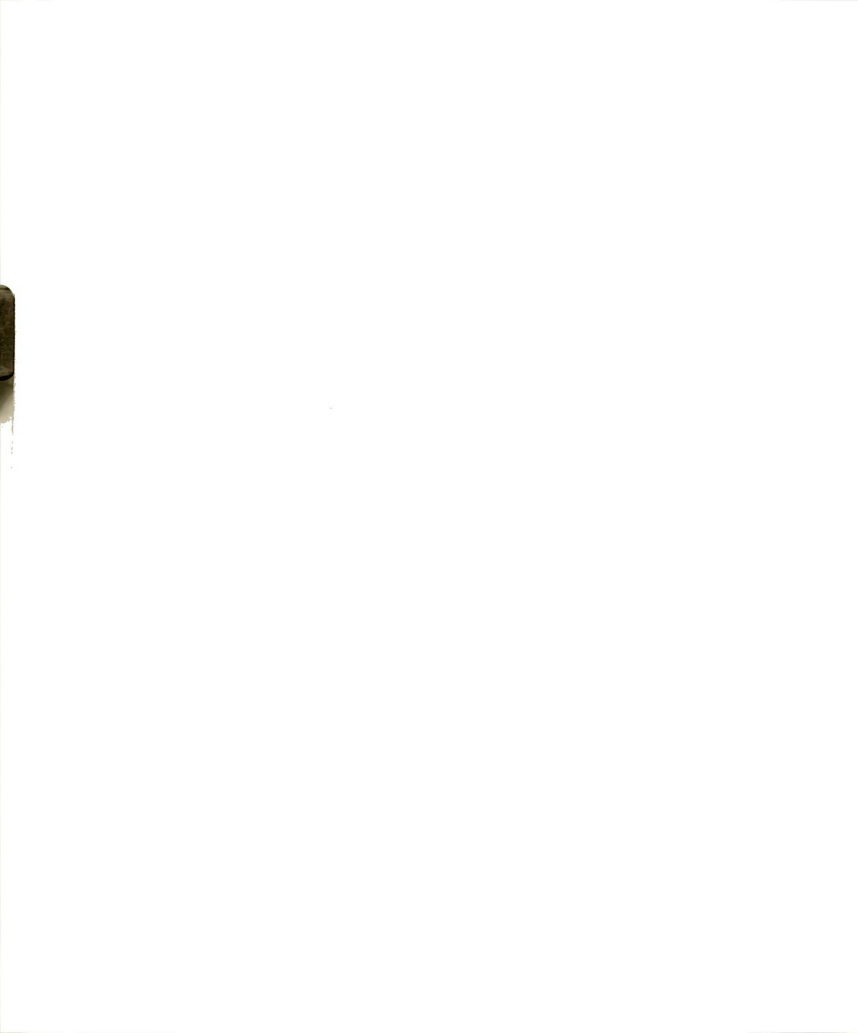
Measuring the acoustic impedance of a boundary is important since the acoustic response of any acoustic system is governed by the acoustic impedance of its boundaries. Accurate mathematical models of acoustic systems require accurate measurements of acoustic impedance. The acoustic impedance of boundaries determines the magnitude and frequency of resonant peaks and the spatial distribution of acoustic response.

A variety of acoustic impedance measurement techniques have been developed in the past. The first techniques used an impedance tube and a single microphone (Hall, 1939; Beranek, 1940; Morse and Ingard, 1968; Dickinson and Doak, 1970; Pierce, 1981). They require measurement of maximum and minimum sound pressure levels at an acoustic resonance in an impedance tube and their spatial locations. These locations and magnitudes are then used to calculate the corresponding impedance (ASTM Standard C 384, 1985a). Identifying the location of maximum and minimum sound pressure levels in an impedance tube is normally difficult and requires physical changes in microphone position. Two of the impedance tube measurement methods (Hall, 1939; Beranek, 1940) use approximate formulas for computing impedance which can also lead to impedance measurement error.

A recent acoustic impedance measurement technique utilizes a two microphone system (Seybert and Ross, 1977; Chung and Blaser, 1980a, 1980b). This technique requires two similar, phase calibrated, microphones at some location in the tube with a

---

\* This chapter is based on the paper "An Eigenvalue Based Acoustic Impedance Measurement Technique," accepted for publication in the *ASME Journal of Vibration and Acoustics*.



known distance between them. The acoustic wave response is then mathematically decomposed into its reflected and incident components using a transfer function between the acoustic pressure at the two microphone locations. The decomposition allows the computation of acoustic impedance (ASTM Standard E 1050, 1985b). ASTM 1050 E, although better than ASTM C 384, requires measurement of the exact distance from the test sample to the center of the nearest microphone and the exact spacing of the microphones. Both these physical dimensions can be difficult to measure accurately. The two microphone method works best with two phase matched microphones and a source whose transfer function has constant magnitude around the frequency of interest. If the microphones are not phase matched, then a correction must be included in the computation of acoustic impedance. These measurement requirements can lead to errors when measuring acoustic impedance using the two microphone technique.

This chapter develops a method for calculating the acoustic impedance based on the eigenvalues of a tube with unknown end impedance. A Fast Fourier analyzer is used to measure complex frequency response from which the eigenvalues of the system are extracted. Acoustic impedance at each resonance is then computed from these eigenvalues. The eigenvalue measurement is independent of microphone position and the location of the response microphone in the tube is arbitrary. The computation of the acoustic impedance from the duct eigenvalues is a closed form solution based on the same plane wave assumptions present in previous methods. The only physical constants required are duct length and the speed of sound in the duct.

#### **4.2. System Model and System Eigenvalues**

The system model is of a one-dimensional hard-walled duct excited by a pressure input at one end and a partially reflective boundary condition at the other end represented by a complex boundary impedance (Chapter 2). The termination end impedance is a ratio

between the pressure and the particle velocity at  $x=L$  and is expressed as (Seto, 1971; Pierce, 1981; Spiekermann and Radcliffe, 1988)

$$\frac{\partial u}{\partial x}(L, t) = -K \left( \frac{1}{c} \right) \frac{\partial u}{\partial t}(L, t) \quad . \quad (4.1)$$

Implicit in (4.1) is the acoustic analogy with electrical systems in which volume velocity is analogous to current and duct pressure is analogous to voltage. A second formulation called the reciprocal acoustic mobility analogy is also sometimes used; and if applied to this system, the parameter  $K$  in (4.1) would be the acoustic admittance. The linear second order wave equation modeling particle displacement in a hard-walled, one-dimensional duct is (Seto, 1971; Doak, 1973)

$$\frac{\partial^2 u(x, t)}{\partial t^2} - c^2 \frac{\partial^2 u(x, t)}{\partial x^2} = - \frac{\partial}{\partial x} \left[ \frac{\delta(x) P_e(t)}{\rho} \right] \quad . \quad (4.2)$$

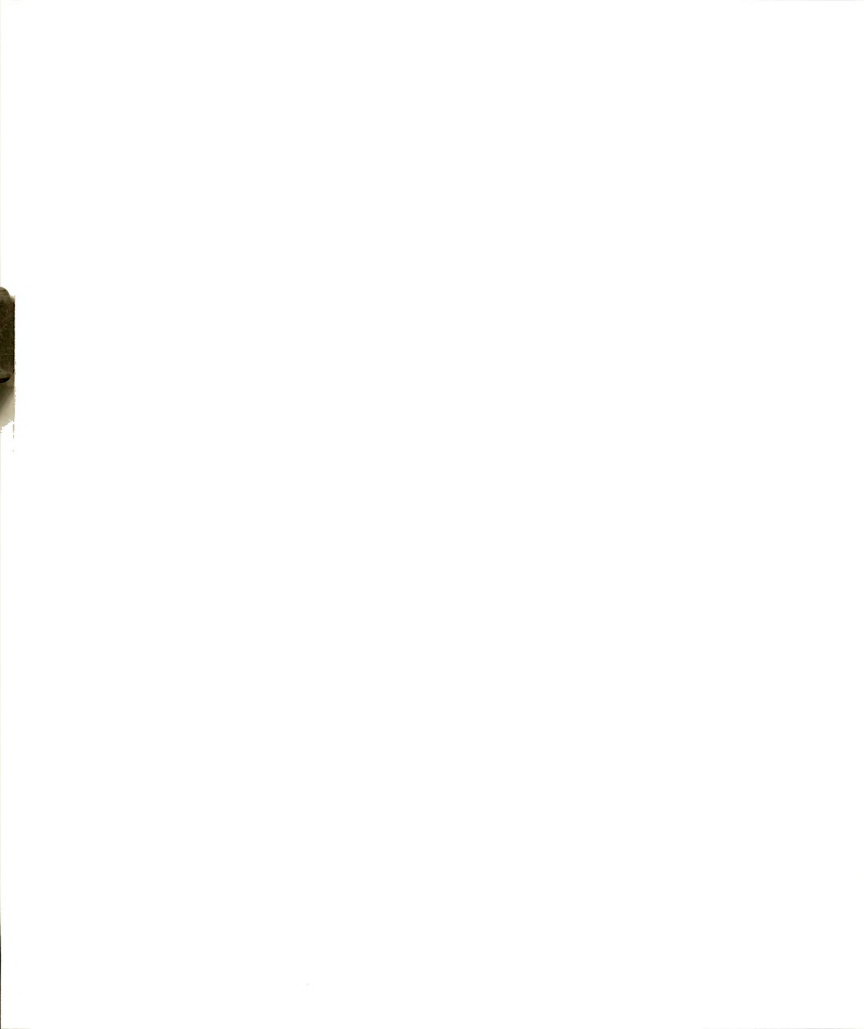
The one-dimensional assumption is usually valid when  $f < 0.586(c/d)$  where  $f$  is the frequency (Hertz) and  $d$  is the diameter of the tube (m) (Annual Book of ASTM Standards, 1985a; 1985b). The duct end at  $x=0$  is modeled as a totally reflective, open end. This boundary condition is (Seto, 1971)

$$\frac{\partial u}{\partial x}(0, t) = 0 \quad . \quad (4.3)$$

This corresponds to an open duct end (or electrical short circuit). Equation (4.3) along with the right hand side of (4.2) model the speaker as a pressure source at  $x=0$ . Implicit in (4.3) is the assumption the source impedance is negligible. If the source impedance is not small, it can be incorporated into the model (Swanson, 1988). The acoustic pressure of the system is related to the spatial gradient of the particle displacement by (Seto, 1971)

$$P(x, t) = -\rho c^2 \frac{\partial u}{\partial x}(x, t) \quad . \quad (4.4)$$





The separation constants of the model were found in Chapter 2. They are

$$\lambda_n = \frac{1}{2L} \log_e \left( \frac{1-K}{1+K} \right) - \frac{n\pi i}{L}, \quad n = 0, \pm 1, \pm 2, \dots \quad (4.5)$$

The system eigenvalues  $\Lambda_n$  are equal to the separation constant multiplied by the wave speed  $c$  ( $\Lambda_n = c\lambda_n$ ). An eigenvalue plot is shown in Figure 4.1. These eigenvalues are each functions of acoustic impedance,  $K$ . The inverse function will allow impedance,  $K$ , to be computed from measured eigenvalues.

### 4.3. Acoustic Impedance Computation

The acoustic impedance  $K$  of the end can be determined at each duct resonance from the eigenvalue at that resonance. This computation assumes the eigenvalues of the system are known. Measuring these duct system eigenvalues is discussed in the next section. Directly solving for  $K$  in terms of  $\Lambda$  is very difficult, therefore an intermediate variable  $\beta$  is introduced to simplify the acoustic impedance computation. The variable  $\beta_n$  is related to the  $n$ th eigenvalue  $\Lambda_n$  from equation (4.5) as

$$\text{Re}(\Lambda_n) + i \text{Im}(\Lambda_n) = \frac{c}{2L} \log_e [\text{Re}(\beta_n) + i \text{Im}(\beta_n)] - \frac{n\pi ci}{L} \quad (4.6)$$

where  $\text{Re}(\ )$  denotes the real part,  $\text{Im}(\ )$  denotes the imaginary part, and the subscript “ $n$ ” denotes the  $n$ th term. Equation (4.6) is now broken into two parts, one equating the real coefficients and the other equating the imaginary coefficients. The complex logarithm on the right hand side is rewritten as

$$\log_e [\text{Re}(\beta_n) + i \text{Im}(\beta_n)] = \log_e |\beta_n| + i \arg(\beta_n) \quad (4.7)$$

where  $|\beta_n|$  is the magnitude of  $\beta_n$  and  $\arg(\beta_n)$  is the argument of  $\beta_n$ , i.e., the arctangent of  $[\text{Im}(\beta_n)/\text{Re}(\beta_n)]$ .



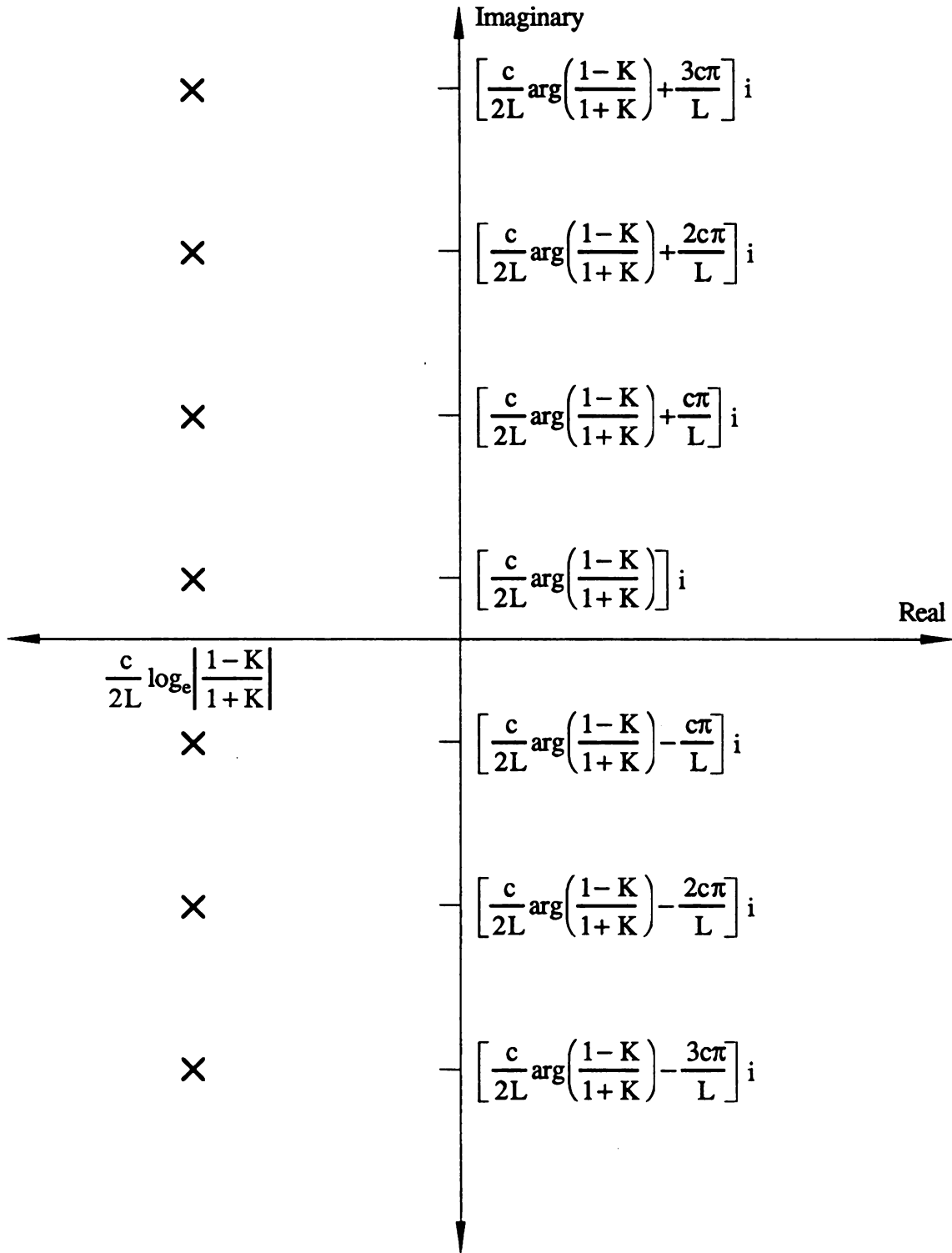
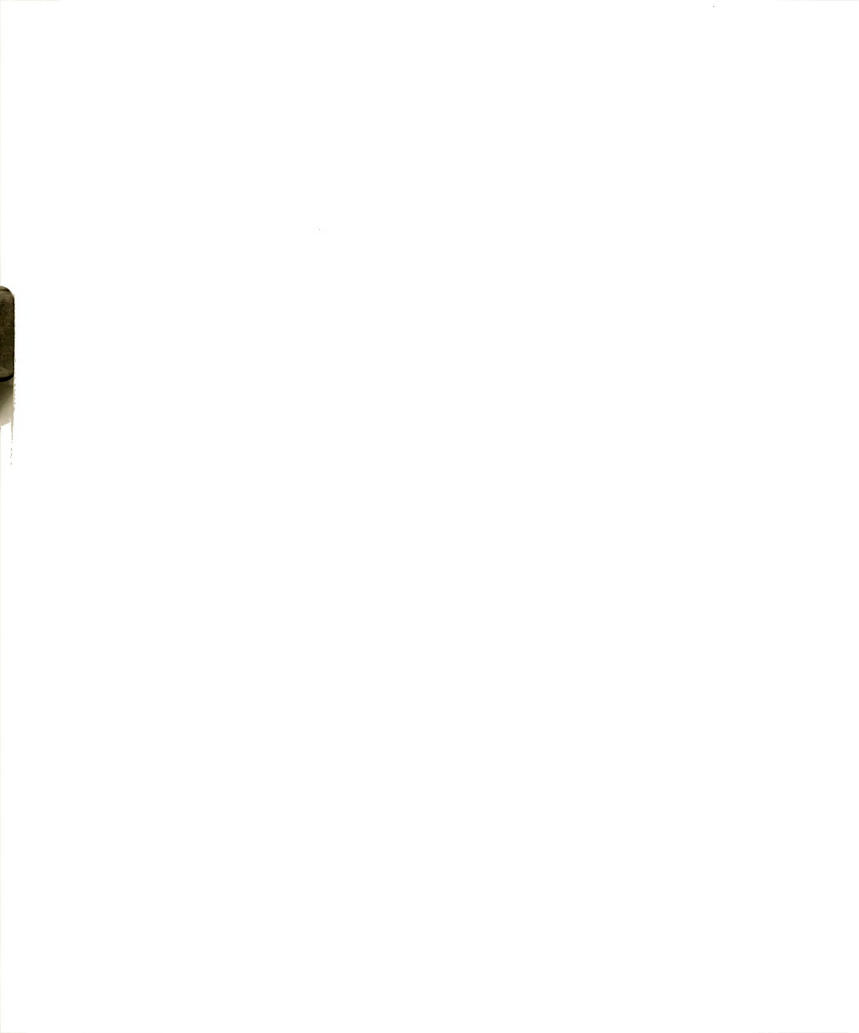


Figure 4.1. System Eigenvalues  $\Lambda_n$ , for Constant  $K$ .



The intermediate variable  $\beta_n$  is now solved for in terms of the real and imaginary parts of the eigenvalues. The real part of  $\beta_n$  is

$$\text{Re}(\beta_n) = \pm \left[ \frac{\exp\left(\frac{4L \text{Re}(\Lambda_n)}{c}\right)}{1 + \tan^2\left(\frac{2Ld_n}{c}\right)} \right]^{\frac{1}{2}} \quad (4.8a)$$

$$\text{where } d_n = \text{Im}(\Lambda_n) + \frac{nc\pi}{L}.$$

The sign of  $\text{Re}(\beta_n)$  in (4.8a) is determined by

$$\text{sgn}[\text{Re}(\beta_n)] = \begin{cases} +1 & \text{if } 0 \leq |\Delta| \leq 0.25 \\ -1 & \text{if } 0.25 < |\Delta| \leq 0.50 \end{cases} \quad (4.8b)$$

$$\text{where } \Delta = \frac{d_n}{\left(\frac{c\pi}{L}\right)}.$$

If the value of  $\Delta$  is less than -0.5 or greater than 0.5, the eigenvalue index  $n$  is incorrect and corresponds to an eigenvalue other than the  $n$ th one. The value,  $n$ , must then be changed to produce a  $\Delta$  between -0.5 and 0.5 which will correspond to the correct eigenvalue index. Once  $\text{Re}(\beta_n)$  is found,  $\text{Im}(\beta_n)$  is found by the equation

$$\text{Im}(\beta_n) = \text{Re}(\beta_n) \tan\left(\frac{2Ld_n}{c}\right) \quad (4.9)$$

where  $\text{Re}(\beta_n)$  is given in (4.8).

The term  $(1-K)/(1+K)$  is now equated to the intermediate variable  $\beta_n$  using (4.5) and (4.6) as



$$\text{Re}(\beta_n) + i \text{Im}(\beta_n) = \frac{1 - \text{Re}(K_n) - i \text{Im}(K_n)}{1 + \text{Re}(K_n) + i \text{Im}(K_n)} \quad (4.10)$$

where  $\text{Re}(K_n)$  is the real part of  $K$  and  $\text{Im}(K_n)$  is the imaginary part of  $K$  for the  $n$ th eigenvalue. Breaking (4.10) into two equations, and solving for  $K_n$  as a function of  $\beta_n$  yields the acoustic impedance as

$$\text{Re}(K_n) = \frac{1 - [\text{Re}(\beta_n)]^2 - [\text{Im}(\beta_n)]^2}{[\text{Re}(\beta_n) + 1]^2 + [\text{Im}(\beta_n)]^2} \quad (4.11)$$

$$\text{Im}(K_n) = \frac{-2 \text{Im}(\beta_n)}{[\text{Re}(\beta_n) + 1]^2 + [\text{Im}(\beta_n)]^2} \quad (4.12)$$

Acoustic impedance measurement  $K_n$  represents the acoustic impedance at the  $n$ th resonant frequency.

#### 4.4. Acoustic Impedance Measurement Experiment

The viability of the above acoustic impedance method was investigated through laboratory tests. The test used a 0.0762 m (3 in) circular PVC schedule 40 duct that was 2.94 m (9.65 ft) long driven by a 0.254 m (10 in) diameter speaker (Realistic 40-1331B). The impedance of a piece of 30 mm thick packing foam inserted in the termination end was tested. The packing foam will be shown to have acoustic impedance which is nearly constant with frequency (Table 4.2), allowing for frequency response comparison to known theory. Speaker input pressure was measured in the exit plane of the input speaker with a Bruel and Kjaer Type 4166 half inch microphone (input reference microphone) attached to a Hewlett Packard 5423A digital signal analyzer. The response of the tube was measured at various locations with another Bruel and Kjaer Type 4166 half inch microphone (response measurement microphone) attached to the signal analyzer (Figure 4.2). Both microphones were calibrated using a Bruel and Kjaer Type 4230 Sound Level Calibrator.





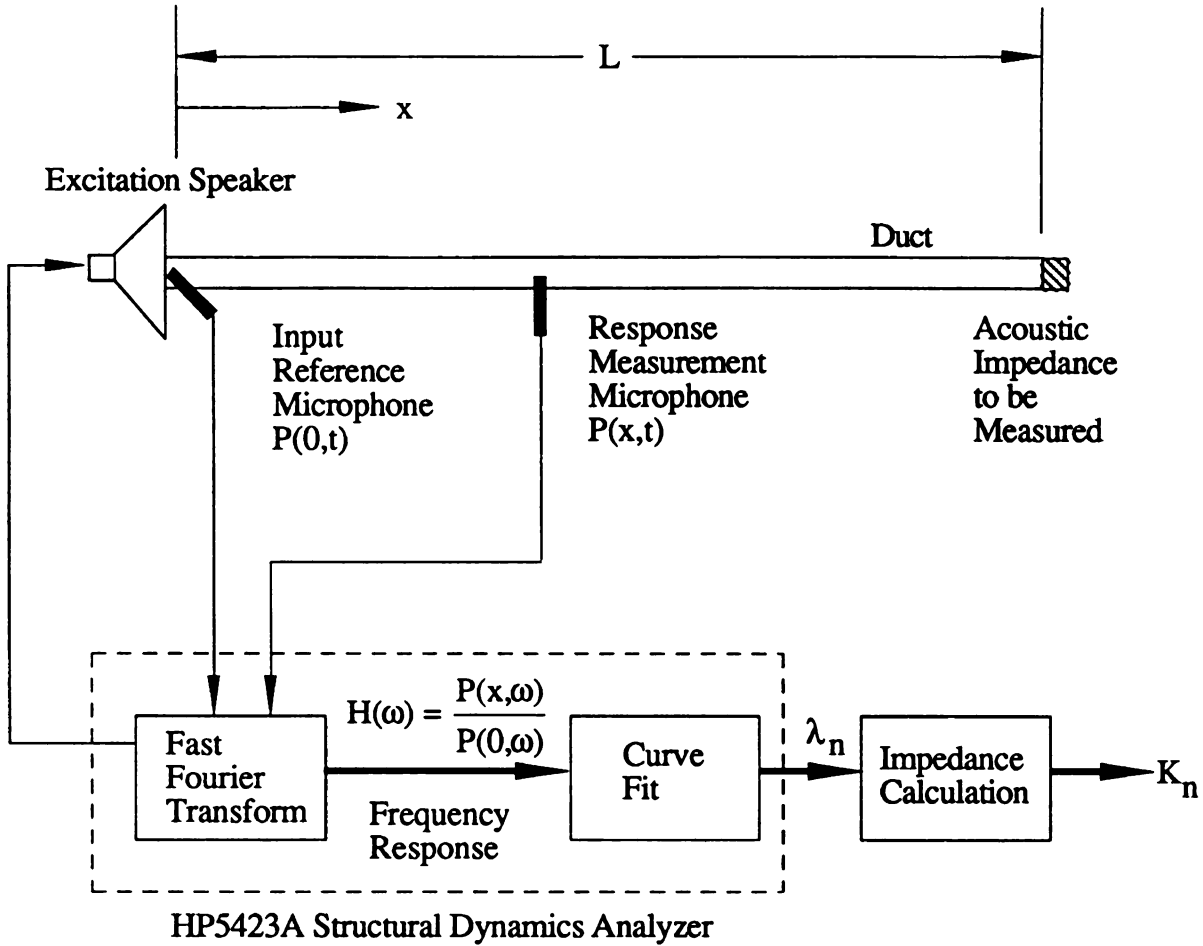


Figure 4.2. Laboratory Configuration.

The impedance measurement technique developed here does not require phase matched microphones nor does it require compensation for phase mismatched microphones. Phase mismatch in the microphones is neglected since the measurements are made at a duct resonant frequency, i.e. the measurements are made when the system phase angles are changing rapidly through 180 degrees. Microphones operating under 500 Hertz rarely have phase error greater than 5 degrees (Bruel and Kjaer, 1982). Steady state eigenvalue measurements are amplitude dominated. The distance between the microphones is not critical, since the duct eigenvalues are independent of measurement location. This is unlike previous methods (Seybert and Ross, 1977; Chung and Blaser, 1980a, 1980b)

where microphone spacing is a required parameter in the analysis and phase matched microphones (or a compensation function) are necessary because wave propagation across the microphones is detected. Errors in the method developed here are only a function of errors associated with measuring the eigenvalues of the duct, the duct length, and the speed of sound. The computation of acoustic impedance from duct eigenvalues is a closed form solution. The method uses the input microphone as an amplitude reference and the excitation speaker does not require a flat response around the frequency of interest, because the response is normalized by the pressure input reference when the Fast Fourier Transform is computed.

The 5423A Structural Dynamics Analyzer used here is capable of providing a number of real time analyses including determining the transfer function (frequency response) of a system and calculating the corresponding eigenvalues. The 5423A Structural Dynamics Analyzer does this by curve fitting a single mode vibration model (two first order states) to the experimental data using the following equation (Hewlett Packard, 1979)

$$H(\omega) = \frac{\text{Re}(A_n) + i \text{Im}(A_n)}{i\omega - \text{Re}(\Lambda_n) - i \text{Im}(\Lambda_n)} + \frac{\text{Re}(A_n) - i \text{Im}(A_n)}{i\omega - \text{Re}(\Lambda_n) + i \text{Im}(\Lambda_n)} + B_1 \omega + B_0 \quad (4.13)$$

where  $H(\omega)$  = the transfer function,

$A$  = the system residue, and

$B_1$  and  $B_0$  = compensation constants for overlapping modes.

Included in the single mode vibration model is compensation for other modes which may be overlapping at that particular frequency. During the curve fitting process, the real and imaginary parts of the eigenvalues are calculated. It is beyond the scope of this paper to describe this process, however, there exist additional alternative methods to extract modal parameters from the transfer function of a system (Hewlett Packard, 1979; Structural

Dynamics Research Corporation, 1983). Eigenvalue extraction is a common function of commercial Fast Fourier analyzers.

The first part of the experiment measured the transfer function of the duct with the foam end impedance. The 5423A Structural Dynamics Analyzer does this by sending a random noise signal to the speaker and then computing the ratio of the Fast Fourier Transforms of the input and response signals. Once the transfer function was known, the eigenvalues of the duct were found using the curve fitting process above (4.13). From the eigenvalues, the acoustic impedance of the foam was determined using equations (4.5) - (4.12).

The mean and standard deviation of the measured eigenvalues of the system with the foam end impedance are shown in Table 4.1. These values are derived from five independent sets of measurements at  $x=0.792$  m (2.60 ft) through  $x=1.42$  m (4.67 ft) at 0.157 m (0.52 ft) increments. Each individual eigenvalue was measured from a transfer function composed of 20 averaged Fast Fourier transforms. The calculated acoustic impedance of the foam is shown in Table 4.2. In this case, the real part of the acoustic impedance dominates the response. Figure 4.3 shows the measured frequency response at  $x=0.792$  m (2.60 ft) compared to the theoretical frequency response for  $K=0.273+0.034i$  at the same point. The value of  $P/P_0$  is the ratio of the response to the input and the measured responses are marked by X's while the theoretical response is denoted by a solid line. The impedance,  $K$ , used in the theoretical response is the average of the six individual acoustic impedance measurements taken at different locations along the duct. Figure 4.3 demonstrates that the theoretical model using the measured acoustic impedance of a material can accurately predict duct response. There is a high degree of accuracy in both the magnitude and the phase angles.

The acoustic impedances of the above experiment were calculated by increasing the magnitudes of both the real and imaginary parts of the measured eigenvalues by one, two and three standard deviations from their mean values. After these changes, the magnitude of the calculated impedance  $K$  only changed by an average of 1.7%, 3.2%, and 5.0% respectively. This shows the high stability of the measurement technique, its resistance to error propagation, and the accuracy of acoustic impedances determined using it.

The experiment was repeated for a capped end. The results are shown in Tables 4.3 and 4.4. An ideal closed end would have an impedance of infinity, however, the real material used here has some absorption. The large impedances shown in Table 4.4 indicate this trend and the variation of impedance with frequency in this case. Figure 4.4 shows the measured frequency response compared to a theoretical frequency response calculated using the measured impedances. The theoretical frequency response was produced by assembling a state space model which used the measured acoustic impedances at each eigenvalue. As in Figure 4.3, there is a high degree of accuracy in both the magnitude and phase angles.

It is important to monitor the value of  $\Delta$  when testing extremely reflective ends. It is possible for eigenvalue computation errors to yield a  $\Delta$  greater than 0.50 with the correct index  $n$  for large impedances. From the above measurements, a value of coefficient,  $\Delta=.51$  was calculated for the one of the eigenvalues. Because the measurements were only accurate to two significant figures, the coefficient was rounded to  $\Delta=0.5$ . For most materials the reflectivity is not large enough for this to be a concern.

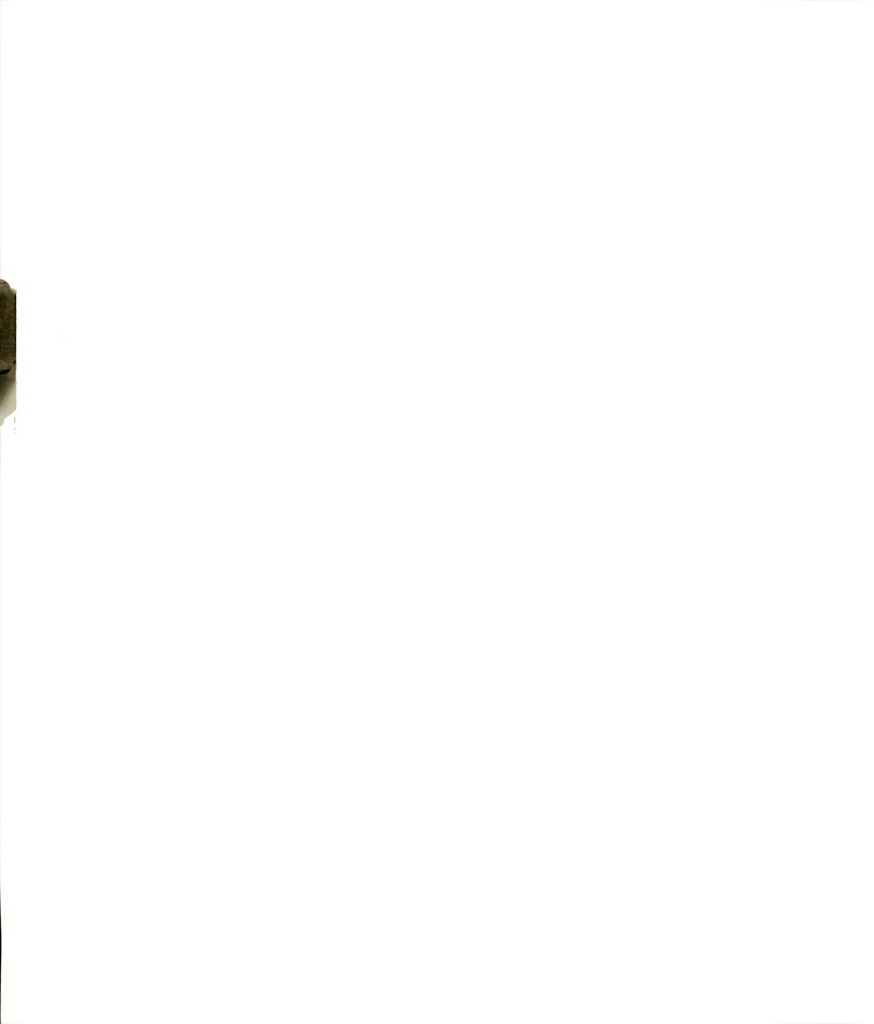


Table 4.1. Measured Duct Eigenvalues for the Foam End.

Eigenvalue (n)	$\text{Re}(\Lambda_n)$ mean, x	$\text{Re}(\Lambda_n)$ std. dev., s	$\text{Im}(\Lambda_n)$ mean, x (Hertz)	$\text{Im}(\Lambda_n)$ std. dev., s (Hertz)
1	-4.955	0.033	57.89	0.045
2	-5.204	0.124	116.3	0.055
3	-5.713	0.091	174.7	0.152
4	-5.755	0.131	233.8	0.259
5	-4.231	0.122	291.7	0.164
6	-5.414	0.117	350.5	0.192

Table 4.2. Calculated Acoustic Impedance for the Foam End.

Eigenvalue (n)	$\text{Re}(K_n)$	$\text{Im}(K_n)$
1	0.260	0.032
2	0.273	0.037
3	0.298	0.042
4	0.300	0.014
5	0.224	0.046
6	0.283	0.031
mean, x	0.273	0.034
std. dev., s	0.028	0.011

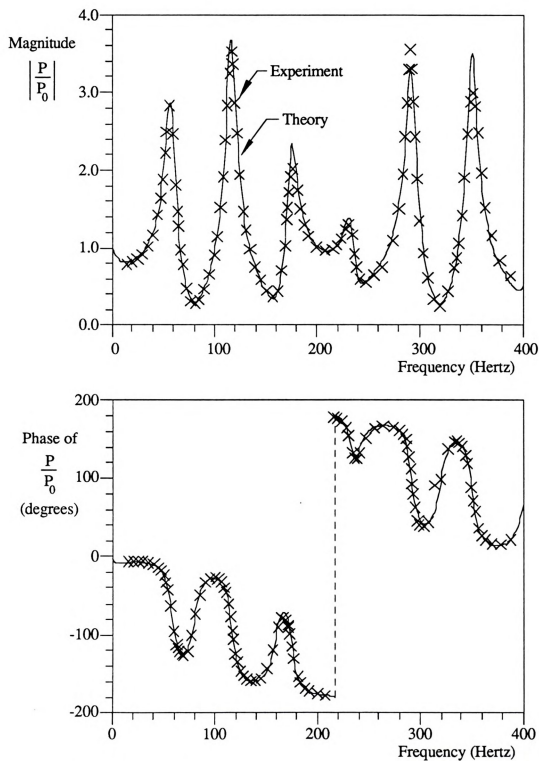


Figure 4.3. Frequency Response of Duct with Foam End at  $x=0.792$  m.



Table 4.3. Measured Duct Eigenvalues for the Capped End.

Eigenvalue (n)	$\text{Re}(\Lambda_n)$	$\text{Im}(\Lambda_n)$ (Hertz)
1	-0.723	29.1
2	-0.847	88.4
3	-1.010	147.2
4	-1.279	206.0
5	-1.419	264.6
6	-0.914	324.1
7	-1.038	381.9

Table 4.4. Calculated Acoustic Impedance for the Capped End.

Eigenvalue (n)	$\text{Re}(K_n)$	$\text{Im}(K_n)$
1	24.37	-5.88
2	15.06	-10.22
3	11.06	-9.03
4	8.54	-7.16
5	8.07	-6.38
6	3.32	-7.47
7	6.81	-8.68

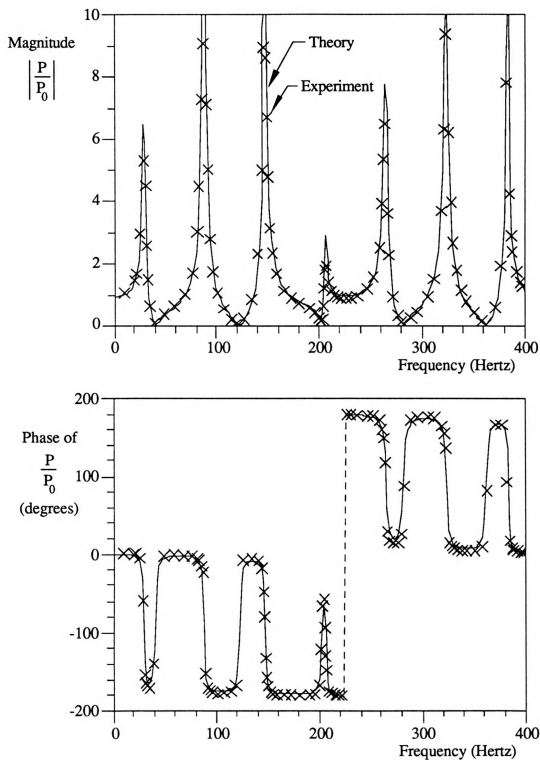


Figure 4.4. Frequency Response of Duct with Closed End at  $x=0.792$  m.



## Chapter 5. State Estimation\*

### 5.1. Introduction

An active noise control system in a duct usually consists of one or more cancellation speakers driven by an algorithm designed to reduce noise levels in the duct. The duct normally has one or more signal microphones at some location while noise is driven by excitation through one end. The goal of the research discussed here is the application of classical pole placement to the problem of active noise control in a duct. Pole placement modifies the eigenstructure of the system to increase the dissipation of the duct and attenuate duct noise. This requires knowledge of the values of the system states. In the previously developed state space duct model (Chapter 2), the system states in the duct are not measurable, and a state estimator must be developed.

The observer is a computer model that runs in parallel with the actual duct system (Luenberger, 1964; Luenberger, 1966) whose input is the input into the actual system plus an error feedback designed to drive the computer model states to values approaching the actual system states. The output of the observer are state estimates and a system pressure estimate. This chapter develops the state estimator (Figures 5.1 and 5.2) for the one-dimensional hard-walled duct with a speaker at some location, a totally reflective entrance boundary condition, and a partially absorptive termination boundary condition. The excitation is a speaker with input signal  $v(t)$  that is independent of the dynamics of the duct.

---

\* This chapter is based on "State Estimation of the Nonself-Adjoint Acoustic Duct System," accepted for publication in the *ASME Journal of Dynamic Systems, Measurement, and Control*.

The next chapter will develop a state space controller to generate  $v(t)$  as a noise control based on state estimates.

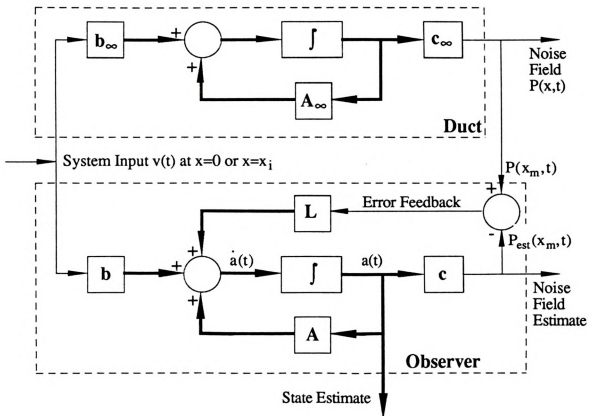


Figure 5.1. Observer and Duct Diagram (Chen, 1984).

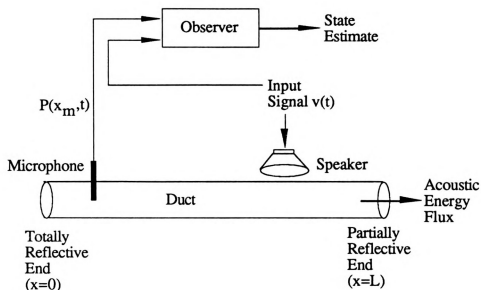


Figure 5.2. Duct with Observer and Input Speaker.

## 5.2. Observer Equations

Typical observer structure is shown in the flow chart in Fig. 5.1. The thick lines represent vector quantities and the thin lines represent scalar quantities. The system input is a mass flow excitation at location  $x=x_i$  in the duct or a pressure excitation at  $x=0$ . The error feedback is the comparison between the actual noise field and the estimated noise field at location  $x=x_m$ . The state estimates, once available, can be passed to a controller to drive a compensator. The control objective is to change the eigenvalues of the system so that the duct is less responsive to external pressure excitation at certain design frequencies.

The duct is an infinite dimensional system. The observer is a finite dimensional system whose order is based on the truncated state space model. When the state space formulation is truncated, the truncated model response only converges to the exact response over a limited frequency range (Chapter 2). Increasing the number of terms  $n$  in the truncated solution increases the frequency bandwidth over which the truncated solution converges to the exact solution. Although many methods have been developed recently to



suppress the errors associated with model truncation (Chait et al., 1988), observation spillover error will always occur when an unmodeled mode in the infinite dimensional system produces an error in the state estimator. The effect of truncation-induced observation spillover errors will be examined below.

The observer equations for a single input are

$$\dot{\mathbf{a}}(t) = [\mathbf{A} - \mathbf{l}\mathbf{c}^T]\mathbf{a}(t) + \mathbf{b}v(t) + \mathbf{l}P_{\text{est}}(x_m, t) \quad (5.1)$$

$$P_{\text{est}}(x, t) = \mathbf{c}^T \mathbf{a}(t) \quad (5.2)$$

where  $P_{\text{est}}(x, t)$  = the observer estimate of the pressure in the duct,  $v(t)$  = the system input,  $\mathbf{b}$  = the input vector (different depending on if the excitation is in the domain or at the end),  $\mathbf{l}$  the observer gain vector, and the superscript  $T$  denotes the matrix transpose. Equations (5.1) and (5.2) are the observer equations for the duct used to provide for a state estimate in the duct when the states are not measurable.

### 5.3. Observer Gain Placement

The observer gains form the vector  $\mathbf{l}$ . Conventional practice is to choose them so that the real part of the eigenvalues of  $\mathbf{A} - \mathbf{l}\mathbf{c}^T$  are two to four times the magnitude of the imaginary part of the eigenvalues of  $\mathbf{A}$  (Franklin and Powell, 1980). The imaginary part of the eigenvalues typically remains unchanged. This practice allows the observer to resonate at the same frequencies as the duct. The algorithm to place the observer gains is listed below.

1. Find the characteristic equation of  $\mathbf{A}$ . This is the determinant of  $[s\mathbf{I} - \mathbf{A}]$  and is written as  $s^n + \alpha_1 s^{n-1} + \alpha_2 s^{n-2} + \alpha_3 s^{n-3} + \dots + \alpha_{n-1} s + \alpha_n$  where the  $\alpha$ 's will be used to



determine 1. The  $\alpha$ 's are related to the eigenvalues of  $\mathbf{A}$  by the elementary symmetric functions

$$\alpha_1 = \sum_{i=1}^n \Lambda_i = \text{trace } \mathbf{A} \quad (\Lambda_i = c\lambda_i)$$

$$\alpha_2 = \sum_{\substack{i=1 \\ i < j}}^n \Lambda_i \Lambda_j = \text{trace}_2 \mathbf{A}$$

$$\alpha_3 = \sum_{\substack{i=1 \\ i < j < k}}^n \Lambda_i \Lambda_j \Lambda_k = \text{trace}_3 \mathbf{A}$$

.

.

.

$$\alpha_n = \prod_{i=1}^n \Lambda_i = \det \mathbf{A} = \text{trace}_n \mathbf{A}$$

2. Find the characteristic equation of  $[\mathbf{A} - c\mathbf{l}^T]$ . This is written as  $s^n + \beta_1 s^{n-1} + \beta_2 s^{n-2} + \beta_3 s^{n-3} + \dots + \beta_{n-1} s + \beta_n = 0$ . The  $\beta$ 's are related to the eigenvalues of  $[\mathbf{A} - c\mathbf{l}^T]$  in the same manner as the  $\alpha$ 's are related to the eigenvalues of  $\mathbf{A}$  above.

3. Define the intermediate observer vector  $\mathbf{l}_1^T$  using the  $\alpha_i$  and  $\beta_i$  derived above.

$$\mathbf{l}_1^T = [\beta_n - \alpha_n \quad \beta_{n-1} - \alpha_{n-1} \quad \dots \quad \beta_2 - \alpha_1 \quad \beta_1 - \alpha_1].$$

4. Form the modal intermediate observation matrix  $\mathbf{T}$ . The columns of  $\mathbf{T}$  are

$$\mathbf{t}_n = \mathbf{c}$$

$$\mathbf{t}_{n-1} = \mathbf{A}\mathbf{c} + \alpha_1 \mathbf{c}$$

$$\mathbf{t}_{n-2} = \mathbf{A}^2 \mathbf{c} + \alpha_1 \mathbf{A}\mathbf{c} + \alpha_2 \mathbf{c}$$

.

.

$$\mathbf{t}_1 = \mathbf{A}^{n-1} \mathbf{c} + \alpha_1 \mathbf{A}^{n-2} \mathbf{c} + \dots + \alpha_{n-1} \mathbf{A}\mathbf{c} + \alpha_n \mathbf{c}$$

and

$$\mathbf{T} = [\mathbf{t}_1 \quad \mathbf{t}_2 \quad \dots \quad \mathbf{t}_{n-1} \quad \mathbf{t}_n].$$

5. Invert  $T$  and find the observer gains by  $l^T = l_1^T T^{-1}$ .

Due to the spectral bandwidth of the  $\Lambda$ 's, the matrix  $T$  is algorithmically singular when  $n > 5$  ( $L = 1.524$  m) for matrix inversion using the International Math and Statistical Libraries (IMSL) linear equation solver with double precision constants. The matrix is column-wise ill conditioned. Using this knowledge, the matrix can be preprocessed (for  $5 < n < 12$ ) by dividing each member of each column by a complex number that has the largest real and imaginary values in that particular column. The modified matrix is then passed to the IMSL linear equation solver and inverted. The inverted matrix is now rescaled, with the rows divided by the above complex number. Using this technique, the matrix  $T$  can be inverted for  $n = 11$ . For  $n > 11$ , the characteristic equations cannot be generated and the matrix  $T$  cannot be constructed on a MicroVAX II. If a computer with more precision is available, the problem can be solved for larger values of  $n$ .

#### 5.4. Closed Form Solution

A closed form solution to (5.1) and (5.2) can be derived by transforming the equations into orthogonal space. This starts by making the substitution

$$a(t) = Uz(t) \quad (5.3)$$

where  $U$  = the eigenvectors of  $[A - lc^T]$  arranged by columns sorted in order of smallest to largest imaginary value of the corresponding eigenvalue. Using this substitution, (5.1) and (5.2) become

$$U \dot{z}(t) = [A - lc^T] Uz(t) + bv(t) + lP(x_m, t) \quad (5.4)$$

$$P_{est}(x, t) = c^T Uz(t) . \quad (5.5)$$

To transform the equations into an orthogonal space, (5.4) is multiplied on the left side by the matrix  $\mathbf{V}^*$ , where  $\mathbf{V}^*$  = the conjugate transpose of the eigenvectors of the conjugate transpose of  $[\mathbf{A} - \mathbf{I}c^T]$  arranged by columns sorted in order of largest to smallest imaginary value of the corresponding eigenvalue. The magnitudes of  $\mathbf{U}$  and  $\mathbf{V}^*$  are based on the orthonormal relationship  $\mathbf{V}^*\mathbf{U} = \mathbf{I}$ . The observer equations in orthogonal space are

$$\mathbf{V}^*\mathbf{U}\dot{\mathbf{z}}(t) = \mathbf{V}^*[\mathbf{A} - \mathbf{I}c^T]\mathbf{U}\mathbf{z}(t) + \mathbf{V}^*[\mathbf{b}v(t) + \mathbf{I}p(x_m, t)] \quad (5.6)$$

or

$$\mathbf{I}\dot{\mathbf{z}}(t) = \mathbf{D}\mathbf{z}(t) + \hat{\mathbf{b}}(t) \quad (5.7)$$

where  $\mathbf{D}$  = the diagonal matrix  $[\Sigma_n]$ ,

$\Sigma_n$  = the observer eigenvalues,

and  $\hat{\mathbf{b}}(t)$  = the vector  $\{\mathbf{V}^*[\mathbf{b}v(t) + \mathbf{I}p(x_m, t)]\}$ .

Equation (5.7) is now composed of decoupled coordinates. The pressure estimate of the observer is obtained by solving for the  $z_n(t)$ 's and inserting them into (5.5). The state estimates are the  $a_n(t)$ 's.

Equations (5.7) and (5.5) were assembled and solved for the case of harmonic excitation. The  $z_n(t)$ 's can be solved for independently as

$$z_n(t) = \left[ z_n(0) - \frac{\tilde{b}_n}{(i\omega - \Sigma_n)} \right] e^{\Sigma_n t} + \left[ \frac{\tilde{b}_n}{(i\omega - \Sigma_n)} \right] e^{i\omega t}, \quad (5.8)$$

where  $\tilde{\mathbf{b}}$  = the vector  $\{\mathbf{V}^*[\mathbf{b} + \mathbf{I}p_s]\}$

and  $P_s$  = steady state amplitude.

The result for a test case of a 5 term observer ( $-2 \leq n \leq 2$ ) and a duct length of 1.52 m (5 ft) is shown in Fig. 5.3. The driving speaker has harmonic excitation at a

frequency of 92.1 Hertz (579 rad/s) and is at location  $x_1=0.305$  m (1 ft). This corresponds to resonance at the  $n=1$  natural frequency. The error feedback is measured at location,  $x=0.610$  m (2 ft). The initial conditions on the  $z(t)$  variables are all zero. The solid line is the real part of the observer pressure and the dashed line is the real part of the duct pressure (equation 5.2) at location 0.762 m (2.5 ft) from the end of the duct. The real part of the pressure is the complex pressure fields image on the real axis. It represents the response a microphone would measure. The duct termination end impedance is  $K=0.25+0.5i$ . Figure 5.3 shows the observer nearly converging to steady state system values after only 3 cycles. This response demonstrates that the observer is operating correctly.

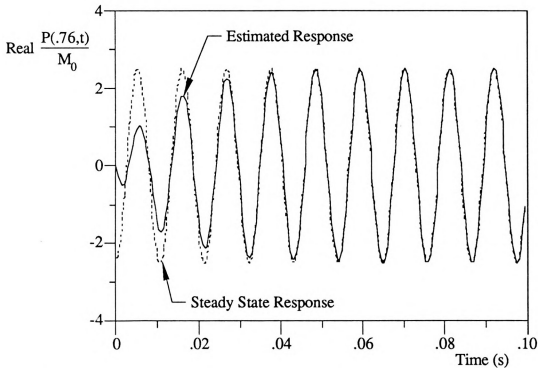


Figure 5.3. Closed Form Solution of Duct Pressure Calculated by Observer Compared with Steady State Duct Model Response.

### 5.5. Numerical Simulations for Continuous Time Observers

Numerical simulations were performed on (5.7) and (5.5) to test for robustness and sensitivity to various integration algorithms. Implementation of a real-time observer requires a stable, noise immune algorithm. Numerical simulations of different algorithms were used to compare the response of three different integration algorithms: the Euler Method, the Runga-Kutta Method, and the Hamming Predictor Corrector General Method. The observer equations were integrated from 0 to 0.1 seconds with varying integration step sizes. The observer parameters were the same as those listed in the Closed Form Solutions section except zero initial conditions were set on acoustic states,  $a(t)$ 's. The numerical integrations were done on a MicroVAX II running a VMS version 4.7 operating system.

The fastest and most stable integration routine was the fourth order Runga-Kutta Integration scheme. Stability was determined by the largest time step the integration algorithm would converge with in this particular problem. The largest step size needed to get a converging value was 0.001 seconds or 100 integration points on the interval  $0 \leq t \leq 0.1$  seconds. The integration required 4.5 seconds from the central processing unit (CPU seconds). Figure 5.4 shows the results of this integration. Although similar to Figure 5.3, Figure 5.4 is an actual system numerically integrated rather than a closed form solution. The solid line is the real part of the observer pressure at  $x=0.762$  m while the dashed line is the real part of the duct pressure at the same location. The integrated observer simulation converges to the correct values in the same number of cycles as the closed form solution. The Hamming Predictor Corrector General Method was the second most stable integration routine. It converged to the correct values for a maximum step size of 0.0002 seconds or 500 integration points on the interval. This required 12.4 CPU seconds. The least robust integration routine turned out to be the Euler Method. It required a step size of 0.00002 seconds or 5000 integration points on the interval and took 51.3 CPU seconds. This was an expected result since the Euler Method is a first order method.

The observer was next tested for response to initial conditions. This is important if a control scheme is going to attenuate transient noise. The initial conditions of all the  $a(t)$ 's were changed from zero to  $a_n(0)=1+1i$ . The results are shown in Figure 5.5. The integration scheme used was a Fourth Order Runge-Kutta Method with a step size of 0.001 seconds. The observer converges to the system values after 0.1 seconds. The response changes by over 4 magnitudes in approximately 100 integration steps. Increasing the values of the initial conditions by 10 ( $a_n(0)=10+10i$ ) requires only two additional cycles for the observer to converge to the system values.

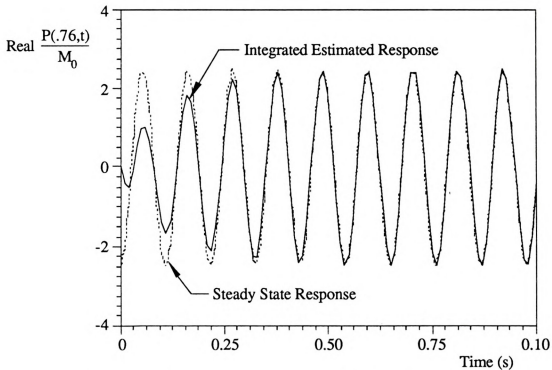


Figure 5.4. Integrated Observer Solution and Model Duct Response.

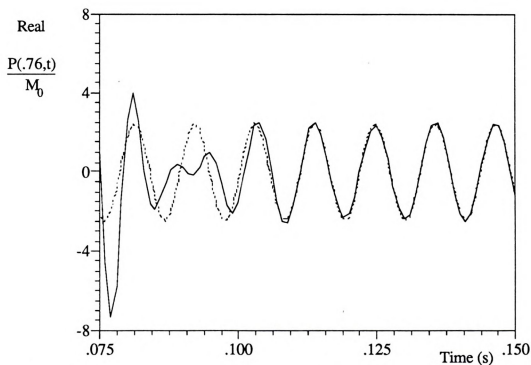
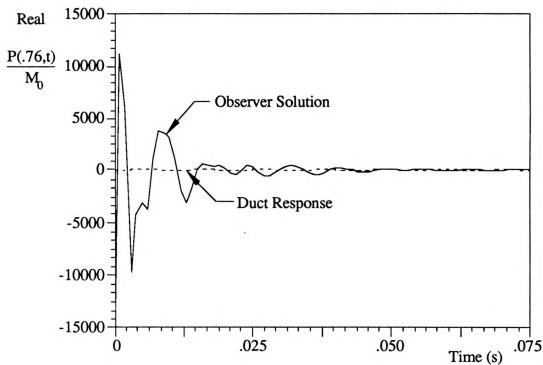


Figure 5.5. Integrated Observer Solution and Model Duct Response.  
Nonzero Initial Conditions Showing Robustness of Observer Design.

Numerical simulations suggest the observer requires one state to model zero frequency response plus two states per duct resonance. For the simulations shown previously, a three term observer will give the same response since the excitation frequency is at  $n=1$ . Nonresonant excitation behaves in a similar manner. If the duct were excited between the  $n=1$  and the  $n=2$  natural frequencies, then a five term observer is typically necessary for reasonable accuracy.

A state estimate is shown in Fig. 5.6. This corresponds to integrated solutions for zero initial conditions on the  $a_n(t)$ 's. The integration method used is the fourth order Runge-Kutta scheme. The state estimate shown is  $a_1(t)$ . The solid line is the real part and the dashed line is the imaginary part. The first state was chosen here because the model is being forced at its first natural frequency and the first state is dominating the response. The first state reaches steady state response after approximately 0.025 seconds.

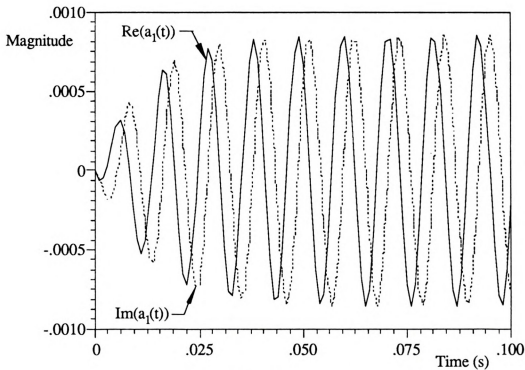


Figure 5.6. State Estimate  $a_1(t)$ .



Truncation induced spillover for the observer and duct only occur if the frequency of the excitation speaker is greater than the bandwidth of the observer. The bandwidth of the observer is equal to the imaginary part of the largest eigenvalue. When this occurs, it produces an unmodeled mode in the duct and as a result the observer cannot converge to the duct values. This problem is avoided if the bandwidth of the observer is larger than the excitation frequency. This is desirable behavior by the observer since it is explicit when the observer will and will not converge. This result is derived from the diagonal state space model formulation (Chait et al., 1988).

## 5.6. Numerical Simulations for a Discrete Time Observer

A faster observer than the continuous observers listed above is a discrete time observer. This was investigated since any real-time control system will have to operate extremely fast to control noise propagating at the speed of sound. To get the discrete time equations, the continuous time equations (5.1) have to be transformed into discrete time. The transformation of equation (5.1) into discrete time is (Ogata, 1970)

$$\mathbf{a}(\mathbf{k} + 1) = \mathbf{F}(\mathbf{T})\mathbf{a}(\mathbf{k}) + \mathbf{g}(\mathbf{T})\mathbf{v}(\mathbf{t}) + \mathbf{h}(\mathbf{T})\mathbf{P}(\mathbf{x}_m, \mathbf{t}) \quad (5.8)$$

where the matrix  $\mathbf{F}(\mathbf{T})$  and the vectors  $\mathbf{g}(\mathbf{T})$  and  $\mathbf{h}(\mathbf{T})$  are dependent on the sampling period  $\mathbf{T}$ . When the sampling period is fixed,  $\mathbf{F}(\mathbf{T})$ ,  $\mathbf{g}(\mathbf{T})$ , and  $\mathbf{h}(\mathbf{T})$  are constant. The matrices  $\mathbf{F}$ ,  $\mathbf{g}$ , and  $\mathbf{h}$  are found by solving the continuous time differential equations then transforming the solution into discrete time (Ogata, 1970). They are

$$\mathbf{F}(\mathbf{T}) = \mathbf{e}^{\mathbf{A}\mathbf{T}} \quad (5.9)$$

$$\mathbf{g}(\mathbf{T}) = \left( \int_0^{\mathbf{T}} \mathbf{e}^{\mathbf{A}\mathbf{t}} \mathbf{d}\mathbf{t} \right) \mathbf{b} \quad (5.10)$$

$$\mathbf{h}(\mathbf{T}) = \left( \int_0^T \mathbf{e}^{\mathbf{A}t} dt \right) \mathbf{I} \quad (5.11)$$

where  $\mathbf{A}$ ,  $\mathbf{b}$ , and  $\mathbf{I}$  are from (5.1). Equations (5.9), (5.10) and (5.11) can be solved for on a digital computer by

$$\mathbf{F}(\mathbf{T}) = \text{InvLap}[(s\mathbf{I} - \mathbf{A})^{-1}] = \sum_{m=0}^{\infty} \left( \frac{\mathbf{A}^m \mathbf{T}^m}{m!} \right) \approx \sum_{m=0}^M \left( \frac{\mathbf{A}^m \mathbf{T}^m}{m!} \right) \quad (5.12)$$

$$\mathbf{g}(\mathbf{T}) = \sum_{m=0}^{\infty} \left( \frac{\mathbf{A}^m \mathbf{T}^{m+1}}{(m+1)!} \right) \mathbf{b} \approx \sum_{m=0}^M \left( \frac{\mathbf{A}^m \mathbf{T}^{m+1}}{(m+1)!} \right) \mathbf{b} \quad (5.13)$$

$$\mathbf{h}(\mathbf{T}) = \sum_{m=0}^{\infty} \left( \frac{\mathbf{A}^m \mathbf{T}^{m+1}}{(m+1)!} \right) \mathbf{I} \approx \sum_{m=0}^M \left( \frac{\mathbf{A}^m \mathbf{T}^{m+1}}{(m+1)!} \right) \mathbf{I} \quad (5.14)$$

where InvLap denotes the inverse Laplace Transform, and  $M+1$  is the number of truncated terms used to form the solution. Once the discrete time equations are solved, the pressure at time  $t$  is found by the equation

$$P_{\text{est}}(x, t) = \mathbf{c}^T \mathbf{a}(\mathbf{k} + \mathbf{I}) \quad (5.15)$$

A discrete time observer simulation was performed on the system described in Section 5.5. Figure 5.7 is a plot of the results. The estimated pressure nearly matches the actual pressure, except for a slight phase shift (time delay) associated with the sampling rate. The simulation took 1.1 CPU seconds on a MicroVAX II using a step size of  $T=0.001$  seconds, which is 75% faster than the fastest continuous observer. The faster time is a result of the integration being done before the matrices are formed, i.e., the integration doesn't have to be executed on-line or in real time. Changing the initial conditions to  $\mathbf{a}_n(0)=1+\mathbf{i}$  produces results similar to Figure 5.5.

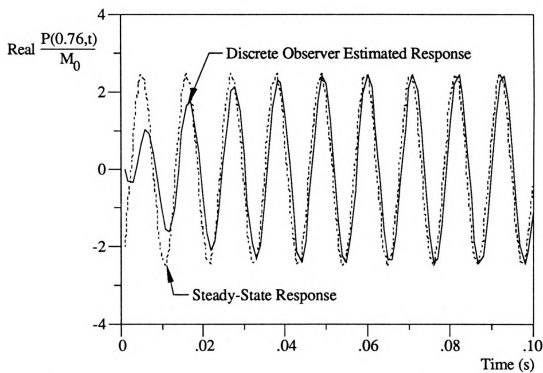


Figure 5.7. Discrete Time Observer Solution and Model Duct Response.

## Chapter 6. Active Noise Control\*

### 6.1. Active Noise Control Using Pole Placement

The control objective is to change the eigenvalues of the system so that the duct is less responsive to external pressure excitations (disturbances) at certain design frequencies. This is done by placing the closed loop system poles to the left of the open loop system poles in the complex plane to enhance the systems stability. Guaranteeing the stability of an infinite dimensional system over an infinite disturbance bandwidth is not possible with truncated state space models. When controlling a finite number of modes in an infinite dimensional system, the problem of an uncontrolled mode going unstable arises. This instability is called control spillover. The closed loop eigenvalues of the acoustic duct can only be placed a reasonable distance to the left of the open loop eigenvalues before an unmodeled mode causes observation or control spillover.

### 6.2. Controller Equations

The control system of the duct is shown in Figure 6.1 and Figure 6.2. The state space equations for the duct with a disturbance speaker and a control speaker are

$$\dot{\mathbf{a}}(t) = \mathbf{A}\mathbf{a}(t) + \mathbf{b}_1 d(t) + \mathbf{b}_2 v(t) \quad (6.1)$$

$$P(x_m, t) = \mathbf{c}^T \mathbf{a}(t) \quad (6.2)$$

---

\* This chapter is based on the paper "Global Active Noise Control of a One-Dimensional Acoustic Duct Using a Feedback Controller," manuscript in preparation, to be submitted to *ASME Journal of Dynamic Systems, Measurement, and Control*.

where  $d(t)$  is the system disturbance and  $v(t)$  is the feedback signal. Placement of the system disturbance on the end is not necessary, however, this corresponds to most industrial problems where a disturbance source excites the duct from one of the ends. The feedback signal is of the form

$$v(t) = -\mathbf{k}\mathbf{a}(t) \quad (6.3)$$

where  $\mathbf{k}$  is the control gain vector. When the observer is added to the system (Figure 6.2), the  $\mathbf{a}(t)$  becomes the observer output,  $\mathbf{a}(t)_{\text{est}}$ .

### 6.3. Control Gain Placement

The controller gains form the vector  $\mathbf{k}$ . They are chosen using the same algorithm used to determine the observer gains  $\mathbf{l}$  (Section 5.3) except that the vector  $\mathbf{c}^T$  is replaced with the vector  $\mathbf{b}$  (Equation 2.23). (The input vector  $\mathbf{b}$  is related to the control gains  $\mathbf{k}$  in the same way the output vector  $\mathbf{c}^T$  is related to the observer gains  $\mathbf{l}$ .)

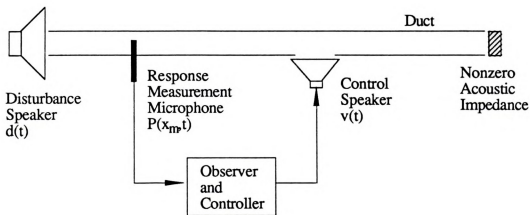


Figure 6.1. Active Noise Control System.

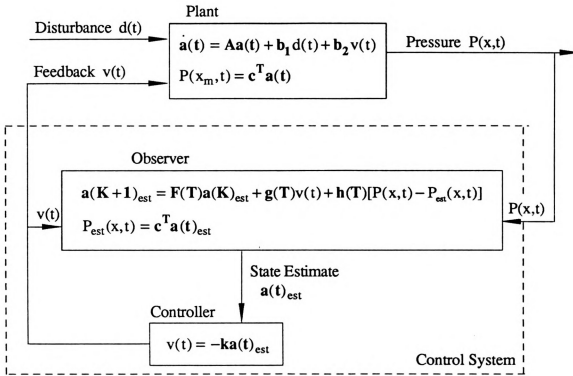


Figure 6.2. Plant and Control System.

#### 6.4. Frequency Domain Simulations

Once the control gains are known, frequency domain simulations can be calculated for (6.1) and (6.2). Frequency domain simulations predict the closed loop steady state response of the system for sinusoidal excitation. The time response of the closed loop system is found by inserting (6.3) into (6.1) which produces

$$\dot{a}(t) = [A - b_2 k]a(t) + b_1 d(t) \quad (6.4)$$

Computing the Laplace transfer of (6.4) produces

$$sa(s) = [A - b_2 k]a(s) + b_1 d(s) \quad (6.5)$$

where (6.5) is in the complex  $s$  plane. Equation (6.5) is solved for at each frequency by letting  $s=i\omega$ , and using the following two definitions

$$d(i\omega) = P_0 e^{i\omega t} \quad (6.6)$$

and

$$a(i\omega) = X e^{i\omega t} \quad (6.7)$$

where  $X$  is, in general, a complex valued vector. Solving for  $X$  yields

$$X = [i\omega I - [A - b_2 k]]^{-1} b_1 P_0 \quad (6.8)$$

The steady state pressure can then be calculated by inserting (6.8) into (6.2). It represents a closed loop system whose eigenstructure has been modified through feedback. The solution to (6.8) assumes that the disturbance dynamics are known and measurable. In general, there is no way to determine the excitation of the duct. The effect of unknown disturbances is discussed in the next section. Additionally, the observer is not included in these frequency domain simulations.

A frequency response of a controlled system is shown in Figure 6.3. The length of the duct is 3.66 m (12.0 ft), the response is measured at  $x=0.792$  m (2.60 ft), and the control speaker is at  $x=3.56$  m (11.69 ft). The acoustic impedance at the end is  $K=0.3+0i$ . The number of terms used to form the model was 11. The solid line is the closed loop response and the dashed line is the open loop response. The real part of the closed loop eigenvalues are twice the magnitude of the open loop eigenvalues. The imaginary part of the eigenvalues remain unchanged. Note that the resonant peaks are all reduced by approximately 50 percent. This is not a generalized result for the placement of the control speaker at any location. Figure 6.4 is a frequency response of the above system with the control speaker at  $x=1.37$  m (4.50 ft). A control speaker placed at this location has little effect on the first mode of the system. Varying the location of the control speaker in

relation to the response measurement and disturbance input has different effects on the system. Numerical simulations show that locating the control speaker near the termination end is the best location for first mode control and a good location for second mode control. They also show that locating the control speaker near the disturbance is a poor location. The eigenstructure of the system can still be modified by placing the control speaker near the disturbance, however, the resulting change in closed loop magnitude response is minimal.

The closed loop poles of the system can also be altered by changing the imaginary part of the open loop eigenvalues. This is useful if the disturbance is occurring at or near an open loop natural frequency. The above system has imaginary eigenvalues at multiples of 47.1 Hertz (296 Rad/sec) for five duct resonances. If there were a disturbance that had harmonics around 141 Hertz (888 Rad/sec), the third mode of the duct would be excited and the response of the system would be large. Figure 6.5 is a plot of the closed loop system with the imaginary part of the third eigenvalue placed at 169 Hertz (1060 Rad/sec). The closed loop pole has increased in amplitude in addition to having its frequency content shifted. If this were a problem, then the real and imaginary parts of the eigenvalues could both be placed. Although the theoretical closed loop eigenvalues can be placed in any location, the actual closed loop eigenvalues can only be moved a reasonable distance from their corresponding open loop values. The further a closed loop pole is moved away from its open loop value, the more likely an unmodeled eigenvalue will create system instability because the high control gains required for a large eigenvalue shift may destabilize unmodeled modes.



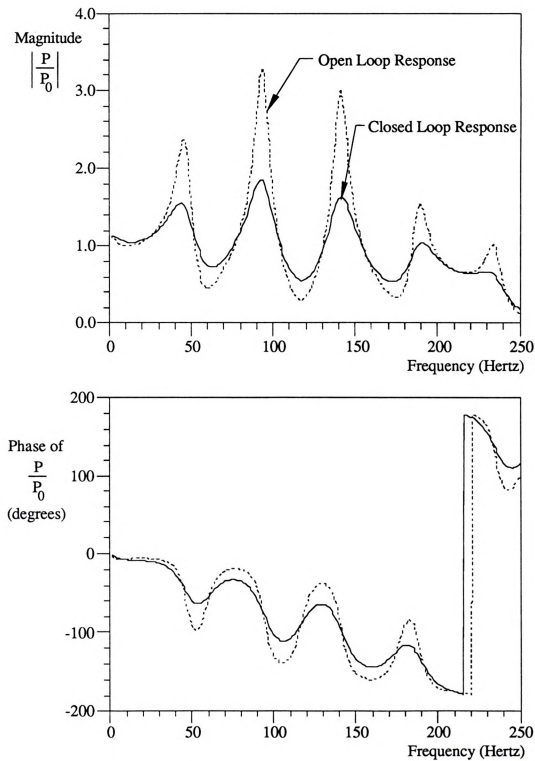


Figure 6.3. Closed and Open Loop Frequency Response, Compensator at 3.56 m.

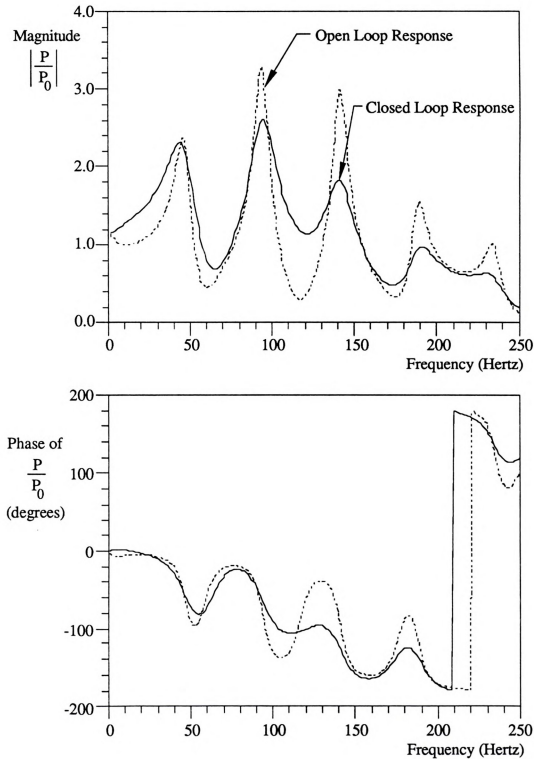


Figure 6.4. Closed and Open Loop Frequency Response, Compensator at 1.37 m.

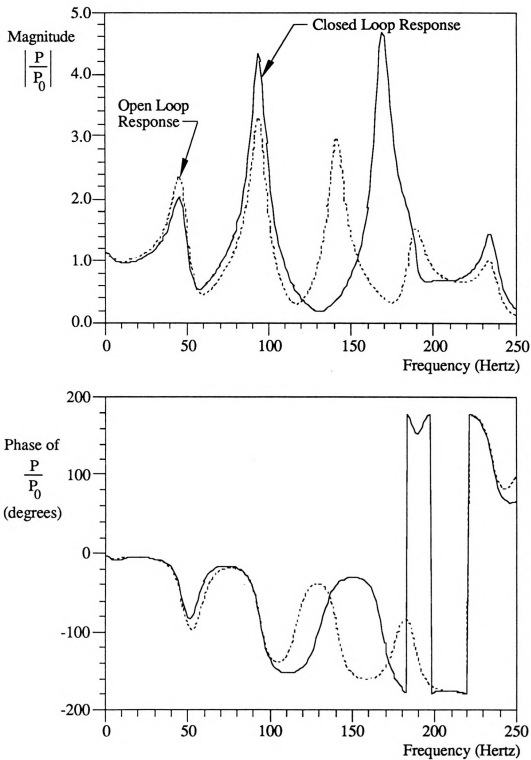


Figure 6.5. Closed and Open Loop Frequency Response, Showing Change of Natural Frequency of System.

### 6.5. Time Domain Simulations

Time domain simulations predict the response of the system over a finite time. They are useful in determining the transient response of the controller and the effects of unmodeled disturbances on the system response. The frequency domain simulations can not include these effects. A computer program modeling the plant and control system (Figure 6.2) was written. It allowed the observer the option to model the disturbance or to leave the disturbance unmodeled. In general, the disturbance is rarely a measurable quantity available to any control system. Analyzing the effects of modeled and unmodeled dynamics in simulation does offer additional insight on system performance and control effectiveness.

A typical time domain simulation is shown in Figures 6.6 and 6.7. The length of the duct is 3.66 m (12 ft), the response is measured at  $x=0.792$  m, (2.60 ft) and the control speaker is at 3.56 m (11.7 ft). The impedance at the termination end was  $K=0.05+0i$ . Five terms were used in the model simulations. The simulation time step size was 0.00005 seconds. The simulation excitation was a sine wave at 47.1 Hertz (296 Rad/sec) which corresponds to the ducts first natural frequency. The observer and controller were both activated at time  $t=0.05$  seconds. Figure 6.6 is the simulation with the disturbance modeled while Figure 6.7 is the simulation with the disturbance unmodeled. In both figures, the solid line is the model duct response while the dashed line is the estimated pressure by the discrete time observer. The steady state value of the simulation with the disturbance known is 6.5 and the steady state value of the simulation with the disturbance unknown is 8.7. Simulations produce similar response for the second mode. These results show that the control action is not as effective if the disturbance is unmodeled.



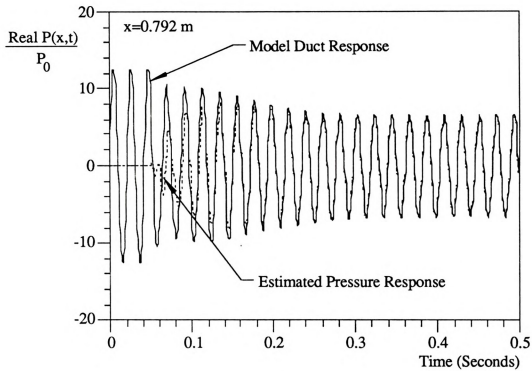


Figure 6.6. Time Domain Response with Modeled Disturbance

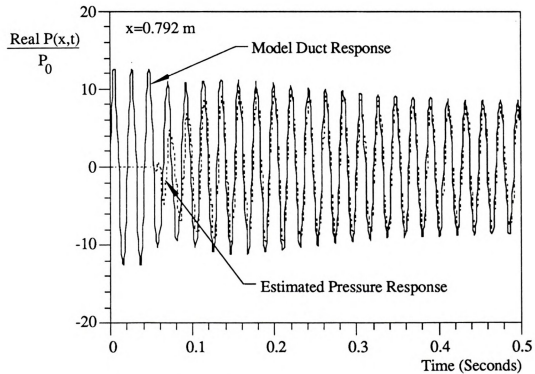


Figure 6.7. Time Domain Response with Unmodeled Disturbance

## 6.6. Actuator Dynamics

The frequency and time domain simulations presented above assume that there are no actuator dynamics. This is not a realistic assumption for control compensators of acoustic systems. The speaker/amplifier actuator system add significant dynamic effects to the control system. This was not a problem in earlier open loop experiments since the input was not the voltage to the speaker, but rather the pressure at the speaker face. It is not possible to ignore the actuator dynamics in the closed loop system since the control system generates a signal that is to be converted into an (unaltered) mass flow.

Figure 6.8 is the magnitude and phase plots of a Bruel and Kjaer Type 2706 power amplifier attached to a 101 mm (4 in) diameter (Realistic 40-1022A) speaker. The mass flow of the speaker was measured with a Bruel and Kjaer Type 3544 helium neon laser velocity measurement system. The velocity of the speaker face is proportional to mass flow. The laser was attached to a Hewlett Packard 5423A digital signal analyzer which measured the values shown in Figure 6.8. The excitation signal was random noise. The X's in the figure are the measured transfer function values and the dashed line is the transfer function for an ideal actuator. Figure 6.8 shows that the transfer function of the actuator is not close to an ideal actuator transfer function.

There are several options to overcome poor actuator dynamics. The first is to design a control system for the actuator itself, using a separate controller. The second is to obtain a number of amplifiers and speakers and test them to determine which has the most ideal characteristics. The third method is to design the closed loop experiment in a way such that actuator dynamics are minimized. This is the method used in the experiment in the next section, choosing a duct length where the first duct natural frequency is around 50 Hertz, an operating region where the actuator has nearly zero phase. This will also provide an actuator bandwidth wide enough for control of the second mode. Control of the third

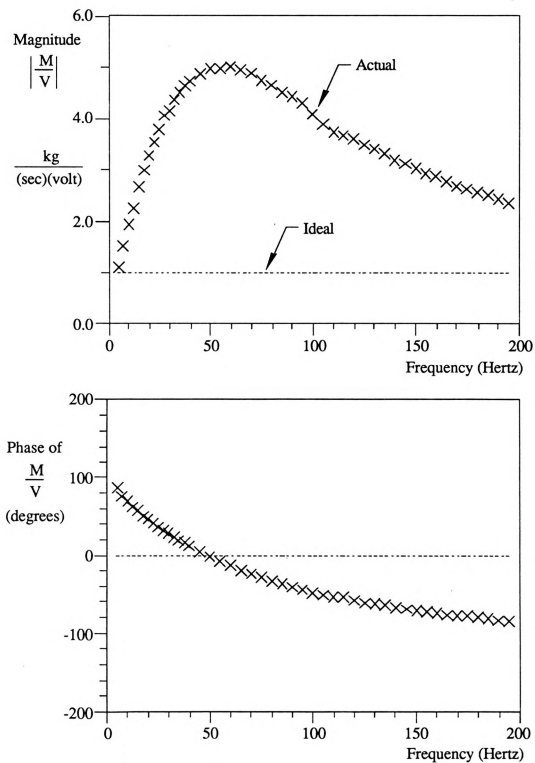


Figure 6.8. Actuator Magnitude and Phase Plots.



mode will not be possible due to the phase angle associated with the actuator at the ducts third natural frequency.

### **6.7. Active Noise Control Experiment**

The duct and active noise control system shown in Figure 6.1 were built using 76 mm (3 in) circular PVC schedule 40 tube that was 3.66 m (12.0 ft) long. The actuator described in section 6.6 was located at 3.56 m (11.7 ft) and the response measurement microphone was a Bruel and Kjaer Type 4166 half inch microphone located at 0.792 m (2.60 ft) from the excitation end. The excitation source was a 254 mm (10 in) diameter speaker (Realistic 40-1331B). The worst case control scenario is an open duct end since it allows the highest pressure levels in the duct of any termination, therefore an open end was chosen. At the open end of the duct, the acoustic impedance was measured to be  $K=0.04+0i$ .

The real time numerical calculations (control system) were run on a Spectral Innovations, Inc. MacDSP64KC digital signal processing (DSP) board that resided in a Macintosh IIX computer. The DSP board is benchmarked at 24 million floating point operations per second (MFLOP). Running a five mode model takes 0.00014 seconds for each data sample, state estimation, control calculation and control output. Attached to the DSP board was a 128000 Hertz data acquisition card with a digital to analog converter and an analog to digital converter. The control system program was written in the C programming language using an AT&T DSP32C C language compiler. Implicit in the compiler is a translation from C to assembly language which allows the DSP board to operate at extremely fast speeds (24 MFLOP) compared to conventional computers such as a MicroVAX or SUN IV.

Acoustic measurements were made with two additional Bruel and Kjaer microphones. The first one was a Type 4166 fixed at the exit plane of the speaker and measured disturbance input pressure. The second one was a Type 4155 and was moved to various locations to measure system response. Both microphones were attached to a Hewlett Packard 5423A digital signal analyzer which measured the transfer function of the system. The excitation of the system was a random noise signal provided by the 5423A signal analyzer. Although periodic signals are available to excite the system, random noise is typical of industrial duct noise. The entire measurement and excitation procedures were independent from the control system. This insured the controller would not be exciting modeled disturbances, which is not a realistic control system.

Due to the actuator dynamics, it is not possible to place the experimental closed loop system poles exactly. However, it is possible to move their real values to the left in the complex plane and obtain a good estimate on where they were placed. This is done by choosing  $k$  such that the closed loop poles are twice the magnitude of the open loop poles. The system model used in the experiment is a five term model (two modes). The gain on the actuator amplifier is then increased to a point where the third mode almost lies on the imaginary axis, or very close to the onset of system instability. The system transfer function is then measured, and the location of the placed pole is calculated from the peak values of the closed loop resonant peaks. This method also shows the maximum peak reduction possible for the described system.

Figures 6.9 and 6.10 are experimental frequency responses at  $x=2.81$  m (9.21 ft). Figure 6.9 is the open and closed loop transfer functions near the first mode and Figure 6.10 is the open and closed loop transfer functions near the second mode of the duct. The boxes denote the open loop response and the X's denote the closed loop response. Although the slight frequency shift of the peaks was not modeled, it has been observed in

the control of mechanical systems (Chait, 1988). The small peak in Figure 6.9 near 55 Hertz is a result of the actuators natural frequency being detected by the measurement instrumentation. Figures 6.11 and 6.12 are plots of the maximum experimental transfer function values versus the length of the duct. Since the method described here is a global noise reduction algorithm, these figures are included to verify that the noise reduction is present everywhere. Figure 6.11 is the open and closed loop maximum values of the first mode. Measurements at 20 locations yield an average attenuation of 58% along the entire duct. Figure 6.12 is the open and closed loop maximum values of the second mode. The average attenuation of the second mode was 55%. From these values, the real part of the closed loop poles were moved approximately three times their open loop values to the left in the complex plane (including compensation for unmodeled dynamics).

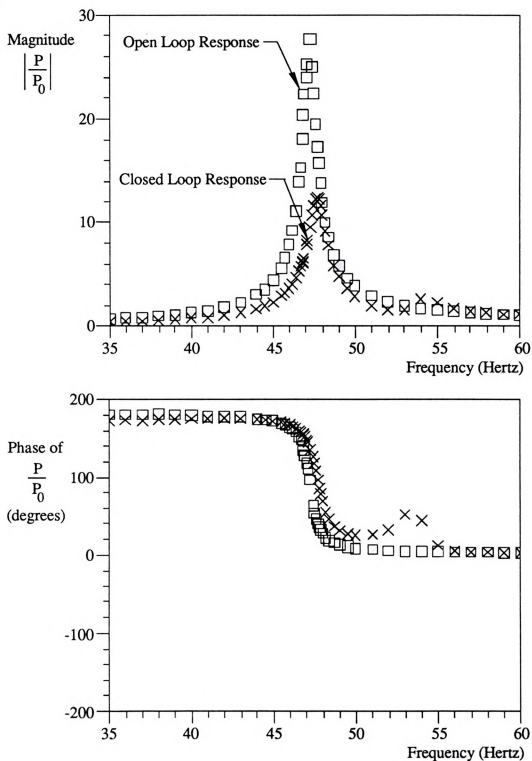


Figure 6.9. Experimental Frequency Response, First Mode.

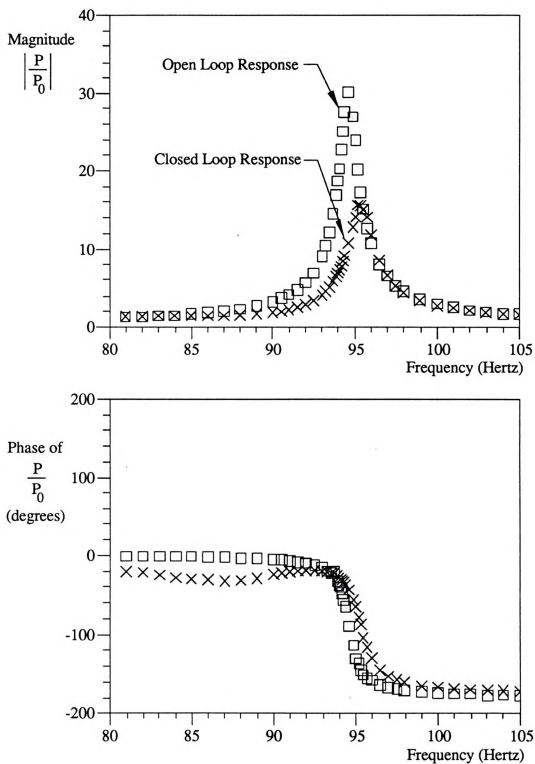


Figure 6.10. Experimental Frequency Response, Second Mode.

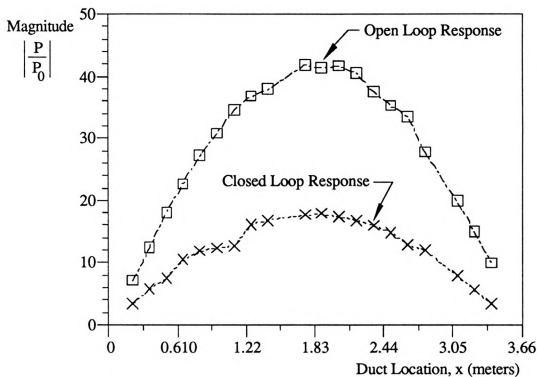


Figure 6.11. First Mode Response.

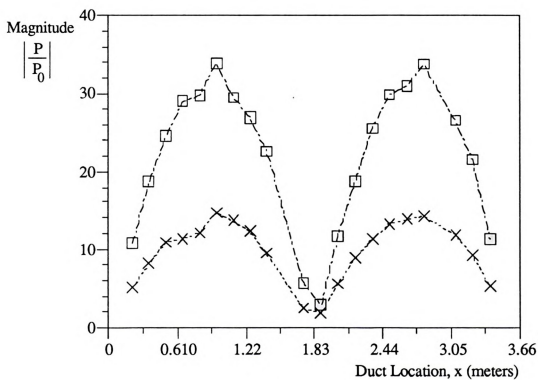


Figure 6.12. Second Mode Response.

## **Chapter 7. Conclusions**

### **7.1. Dissertation Summary**

The dynamic response of an enclosed acoustic system with point impedance on one end can be represented in state space form. A series solution can be implemented to approximate the exact dynamic response. Furthermore, the state space model is diagonal so only a small number of terms are required to get a solution that converges to the exact solution over a limited frequency range. Steady state experiments of pressure excitation and mass flow excitation correlated well with theory. The theory can be used to approximate duct ends that have nonconstant acoustic impedance. The transient response model predicts the measured transient experimental data accurately. The accuracy of the model's transient response is predictably reduced by truncating the model's number of states.

Calculation of the acoustic impedance of a duct end from experimentally obtained impedance tube eigenvalues is developed in this dissertation. These eigenvalues are easily determined from a measured duct transfer function by commercially available Fast Fourier analyzers. This method has the advantage of stationary microphone positioning at any location in the impedance tube. The computational step from eigenvalue to acoustic impedance is a closed form solution. Errors in measured impedance can arise only from errors in measured system eigenvalues, duct length, and the speed of sound. Experimental results show that the method is both accurate and insensitive to measurement errors.

An active noise control technique is developed to globally reduce noise levels. Frequency domain simulations predict that the method will attenuate noise. Time domain

simulations also predict that the technique will attenuate noise and they show the effects of unmodeled disturbances on the system. The dynamic response of control actuators is discussed and the actuators effects are related to the acoustic duct described here. An active noise experiment is demonstrated in which the ducts noise level is reduced globally by 58% for the first mode and 55% for the second mode.

## **7.2. Directions for Future Work**

There are several areas for future work or improvement in the method stated in this dissertation. One of the most obvious extensions would be to move this work into three-dimensional enclosures, since most acoustic systems are three-dimensional rather than one-dimensional. Three-dimensional noise reduction would be extremely useful in aircraft, factories, and other enclosures that requires human habitation. This is a difficult problem since the effects of nonuniform boundary conditions are more prevalent than in a one-dimensional acoustic enclosure.

A topic of improvement in the one-dimensional system is in the area of actuator dynamics. Better actuator dynamics will give better noise control characteristics. A better actuator will also increase the control bandwidth, making control of the third and subsequent modes possible. It might be best to retain the current actuator, and build a separate control unit for the amplifier and speaker which delivers nearly ideal characteristics.

Adding additional sensors and control speakers might also enhance the closed loop systems performance for both the one-dimensional and three-dimensional noise control problem. It would be possible place the system eigenfunctions, rather than its' eigenvalues. This may give better noise attenuation and enhance the closed loop systems stability. One final method noise control method that could be considered is to combine the



pole placement technique with one of the adaptive filter techniques mentioned earlier. The two noise control techniques working together might provide better noise attenuation.

## APPENDIX



## Appendix. Wave Equation Derivation

The derivation of the wave equation is reproduced here. This set of equations can be found in any good acoustics textbook, however some authors formulate the problem using pressure as the independent variable rather than particle displacement.

Consider the one-dimensional duct shown in Figure A.1 of length  $L$  and uniform cross-sectional area  $A$ . The air in the duct is considered to be an ideal gas with density  $\rho$ . The ideal gas assumption requires the temperature to be constant throughout the tube and the air viscosity effects to be negligible. When the duct is excited, the density of the air in any area (of any section) is time variant. Additionally, the density of the air in the duct changes spatially. When the duct is excited, the initial section  $dx$  and instantaneous section  $(dx+du)$  always contain the same mass of air. This results in

$$A\rho dx = A(\rho + d\rho)(dx + du) \quad (A.1)$$

where  $u$  is the instantaneous displacement of any cross section  $dx$  of the enclosure,  $(\rho+d\rho)$  is the instantaneous density of the air, and  $(dx+du)$  is the instantaneous length of the section of air.

Rewriting (A.1) and neglecting the higher order term  $d\rho du$  yields

$$d\rho = -\rho \frac{du}{dx} \quad (A.2)$$

The change of pressure due to the change of volume is expressed as

$$dP = -B \frac{dp}{\rho} \quad (\text{A.3})$$

where  $P$  is the pressure and  $B$  is the bulk modulus of the air. Using (A.2), equation (A.3) can be rewritten as

$$dP = -B \frac{du}{dx} \quad (\text{A.4})$$

When the duct is excited, pressure changes indicated in (A.4) will exert dynamic forces on the section  $dx$ . Balancing the inertia force and the pressure forces on the section results in

$$A\rho dx \frac{d^2u}{dt^2} = A \left( P - B \frac{du}{dx} \right) - A \left( P - B \frac{du}{dx} - B \frac{d^2u}{dx^2} dx \right) \quad (\text{A.5})$$

Equation (A.5) can be simplified, and since the second derivatives of  $u$  are both functions of spatial location  $x$  and time  $t$ , the derivatives are changed to partial derivatives. This equation is

$$\frac{\partial^2 u}{\partial t^2} = c^2 \frac{\partial^2 u}{\partial x^2} \quad (\text{A.6})$$

where  $c^2 = B/\rho$  which is the square of the wave speed in the duct. The excitation the speakers exert on the system can be added to (A.5) on the right hand side as forcing functions on the section.

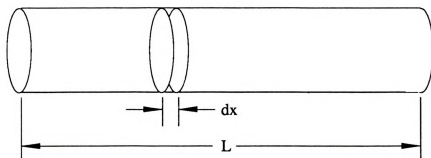


Figure A.1. Duct with Section  $dx$ .

## BIBLIOGRAPHY

## Bibliography

- The American Society for Testing and Materials, 1985a, "Standard Test Method for Impedance and Absorption of Acoustical Materials by the Impedance Tube Method," Annual Book of ASTM Standards, Designation: C 384-85, Vol. 04-06, pp. 144-156.
- The American Society for Testing and Materials, 1985b, "Standard Test Method for Impedance and Absorption of Acoustical Materials Using a Tube, Two Microphones, and a Digital Frequency Analysis System," Annual Book of ASTM Standards, Designation: E 1050-85a, Vol. 04-06, pp. 910-917.
- Bruel and Kjaer, 1982, "Condenser Microphones and Microphone Preamplifiers," Bruel and Kjaer Instruments Inc., Naerum, Denmark.
- Beranek, L.L., 1940, "Acoustic Impedance of Commercial Materials and the Performance of Rectangular Rooms with One Treated Surface," *Journal of the Acoustical Society of America*, Vol. 12, pp. 14-23.
- Chait, Y., 1988, "Frequency Domain Robust Control of Distributed Parameter Systems," Doctoral Dissertation, Michigan State University.
- Chait, Y., Radcliffe, C.J., and MacCluer, C.R., 1988, "Frequency Domain Stability Criterion for Vibration Control of the Bernoulli-Euler Beam," *Journal of Dynamic Systems, Measurement, and Control*, Vol. 110, pp. 303-307.
- Chen, Chi-Tsong, 1984, *Linear System Theory and Design*, Holt, Rinehart and Winston, New York, pp. 324-383.
- Chung, J.Y., and Blaser, D.A., 1980, "Transfer Function Method of Measuring In-Duct Acoustic Properties. I. Theory," *Journal of the Acoustical Society of America*, Vol. 68(3), pp. 907-913.

- Chung, J.Y., and Blaser, D.A., 1980, "Transfer Function Method of Measuring In-Duct Acoustic Properties. II. Experiment," *Journal of the Acoustical Society of America*, Vol. 68(3), pp. 914-921.
- Davis, D.D. Jr., Stokes, G.M., Moore, D., and Stevens, G.L., Jr., 1954, "Theoretical and Experimental Investigation of Mufflers With Comments on Engine Exhaust Design," NACA Report 1192.
- Dickinson, P.J., and Doak, P.E., 1970, "Measurements of the Normal Acoustic Impedance of Ground Surfaces," *Journal of Sound and Vibration*, Vol. 13(3), pp. 309-322.
- Doak, P.E., 1973a, "Excitation, Transmission and Radiation of Sound From Source Distributions in Hard-Walled Ducts of Finite Length (II): The Effects of Duct Length," *Journal of Sound and Vibration*, Vol. 31(2), pp. 137-174.
- Doak, P.E., 1973b, "Excitation, Transmission and Radiation of Sound From Source Distributions in Hard-Walled Ducts of Finite Length (I): The Effects of Duct Cross-Section Geometry and Source Distribution Space-Time Pattern," *Journal of Sound and Vibration*, Vol. 31(1), pp. 1-72.
- Eriksson, L.J., Allie, M.C., Bremigan, C.D., and Gilbert, J.A., 1988, "The Use of Active Noise Control for Industrial Fan Noise," ASME Winter Annual Meeting, Chicago, Paper Number 88-WA/NCA-4.
- Franklin, F.G., and Powell, J.D., 1980, *Digital Control of Dynamic Systems*, Addison-Wesley, Section 6.5.
- Hewlett-Packard, 1979, "User's Guide, 5423A Structural Dynamics Analyzer," Hewlett-Packard Company, Santa Clara, California.
- Kwakernaak, H., and Sivan, R., 1972, *Linear Optimal Control Systems*, John Wiley and Sons, Inc., New York.
- LaFontaine R.F., and Shepherd I.C., 1983, "An Experimental Study of a Broadband Active Noise Attenuator for Cancellation of Random Noise in Ducts," *Journal of Sound and Vibration*, Vol. 91(3), pp. 351-362.



- Luenberger, D.G., 1964, "Observing the State of a Linear System," *IEEE Transactions on Military Electronics*, pp. 74-80.
- Luenberger, D.G., 1966, "Observers of Multivariable Systems," *IEEE Transactions on Automatic Control*, Vol. AC-11, no. 2, pp. 190-197.
- Manjal, M.L., and Eriksson, L.J., 1988, "An Analytical, One-Dimensional, Standing-Wave Model of a Linear Active Noise Control System in a Duct," *Journal of the Acoustical Society of America*, Vol. 84(3), pp. 1086-1093.
- Mollo, C.G., and Bernhard, R.J., 1987, "A Generalized Method for Optimization of Active Noise Controllers in Three-Dimensional Space," AIAA 11th Aeroacoustics Conference, Palo Alto, California, Paper number AIAA-87-2705.
- Morse, P.M., and Ingard, K.U., 1968, *Theoretical Acoustics*, McGraw-Hill Book Company, New York, pp. 469-471.
- Ogata, K., *Modern Control Engineering*, Prentice-Hall, Inc., Englewood Cliffs, N.J., pp. 703-704.
- Pierce, A.D., 1981 *Acoustics: An Introduction to Its Physical Principles and Applications*, McGraw-Hill Book Company, New York, pp. 111-113 and p. 321.
- Rayleigh, J.W.S., 1878, *The Theory of Sound, Volume II*, Dover Publications, New York, pp. 49-68.
- Ross, C.F., 1981, "A Demonstration of Active Control of Broadband Sound," *Journal of Sound and Vibration*, Vol. 74(3), pp. 411-417.
- Roure, A., 1985, "Self-Adaptive Broadband Active Sound Control System," *Journal of Sound and Vibration*, Vol. 101(3), pp. 429-441.
- Seto, William W., 1971, *Theory and Problems of Acoustics*, McGraw-Hill Book Company, New York.
- Seybert, A.F. and Ross, D.F., 1977, "Experimental Determination of Acoustic Properties Using a Two-Microphone Random-Excitation Technique," *Journal of the Acoustical Society of America*, Vol. 61, pp. 1362-1370.

- Snowdon, J.C., 1971, "Mechanical Four Pole Parameters and Their Application," *Journal of Sound and Vibration*, Vol. 15, pp. 307-323.
- Spiekermann, C.E., 1986, "One-Dimensional Acoustic Response with Mixed Boundary Condition: Separating Total Response into Propagating and Standing Wave Components," Doctoral Dissertation, Michigan State University.
- Spiekermann, C.E., and Radcliffe, C.J., 1988a, "Decomposing One-dimensional Acoustic Response into Propagating and Standing Waves," *Journal of the Acoustical Society of America*, Vol. 84(4), pp. 1536-1541.
- Spiekermann, C.E., and Radcliffe, C.J., 1988b, "Stripping One-dimensional Acoustic Response into Propagating and Standing Wave Components," *Journal of the Acoustical Society of America*, Vol. 84(4), pp. 1542-1548.
- Structural Dynamics Research Corporation, 1983, "User Manual for MODAL ANALYSIS 8.0," Structural Dynamics Research Corporation, Milford, Ohio.
- Swanson, D.C., 1988, "The Role of Impedance Coupling in Achieving Global Active Attenuation of Noise," ASME Winter Annual Meeting, Chicago, Paper number 88-WA/NCA-2.
- Swinbanks, M.A., 1973, "The Active Control of Sound Propagation in Long Ducts," *Journal of Sound and Vibration*, Vol. 27(3), pp. 411-436.
- Tichy, J., Warnaka, G.E., and Poole, L.A., 1984, "A Study of Active Control of Noise in Ducts," *Journal of Vibration, Acoustics, Stress, and Reliability in Design*, Vol. 106, pp. 399-404.
- Trinder, M.C.J., and Nelson, P.A., 1983, "Active Noise Control in Finite Length Ducts," *Journal of Sound and Vibration*, Vol. 89(1), pp. 95-105.
- Warner, J.V., Waters, D.E., and Bernhard, R.J., 1988, "Digital Filter Implementation of Local Active Noise Control in a Three Dimensional Enclosure," ASME Winter Annual Meeting, Chicago, Paper number 88-WA/NCA-6.

MICHIGAN STATE UNIV LIBRARIES



31293005856004